

# The Effect of Ozone on Diesel Soot Precursors

Inga L. Faison

Thesis submitted to the Faculty of the  
Virginia Polytechnic Institute and State University  
in partial fulfillment of the requirements for the degree of

Master of Science

in

Mechanical Engineering

Dr. Balakrishnan Ganeshan, Chair

Dr. Uri Vandsburger

Dr. Alan A. Kornhauser

April 23, 1997

Blacksburg, Virginia

Keywords: Combustion, diesel engine, soot precursors, ozone

# The Effect of Ozone on Diesel Soot Precursors

Inga L. Faison

## (ABSTRACT)

A joint experimental and numerical project has been initiated at Virginia Tech to study the effect of ozone on diesel soot precursors. This thesis is the first stage of the numerical part of the project, and contains a study of the effect of the different ozone levels on diesel soot precursors.

This numerical study is executed via the use of two computer programs, Senkin, and PSR. An idealistic model of the diesel engine was used in both analyses. The numerical studies were done at three different engine speeds, 1500, 2000, 2500 RPM and eight different levels of ozone. Studies were performed with ozone introduced with the intake air and with the fuel. Eleven product species, which include dominant soot precursors such as acetylene ( $C_2H_2$ ) and the propargyl radical ( $C_3H_3$ ), were examined and evaluated during this experiment.

After analyzing both simulations, the PSR predictions were not useful since it omits the existence of temperature and species gradients. The PSR analysis was used as a preliminary model to get an overall idea of combustion pollutant formation and predicted the exit soot precursor concentrations were unaffected by any ozone addition. However, the Senkin analysis predicted the ozone injection did have the potential to reduce the formation of soot precursors. The Senkin analysis predicted more realistic results and therefore it is believed to yield the correct conclusion. However, it was suggested that an additional program, such as KIVA3, be utilized to predict a more practical view of the chemical kinetic behavior of ozone and its effect on the diesel engine.

## ACKNOWLEDGMENTS

First of all, I would like to give thanks to God because without his love and grace none of this would have been possible. These are the humble words I have learned to live by: I can do all things through Christ which strengthenth me (Phillipians 4:13).

I would also like to give thanks to my advisor Dr. Balakrishnan Ganeshan for allowing me to work with him on this project. I greatly appreciate his open door policy as well as his knowledge and experience with computational combustion experiments. These attributes were extremely beneficial when problems occurred during my research. He seems to always give the guidance and encouragement that was needed to solve, what at the time seems to be, insurmountable dilemmas.

Last but definitively not least, I would like to thanks my family and friends for their support. I especially want to acknowledge my parents, Louis and Veta Faison. None of this would have been possible without them. They were always there when I needed to vent or to be encouraged when times were rough. My parents' love and understanding revitalized me and helped me to obtain this degree.

## Table of Contents

<b>ABSTRACT</b>	<b>ii</b>
<b>ACKNOWLEDGMENTS</b>	<b>iii</b>
<b>Table of Contents</b>	<b>iv</b>
<b>List of Figures</b>	<b>vi</b>
<b>Chapter 1: Introduction</b>	<b>1</b>
1.1 Previous Work	1
1.1.1 Chemical Kinetic Analysis	2
1.2 Formulation of Initial Conditions	5
1.3 Computational considerations	7
1.4 Motivation	7
<b>Chapter 2: Soot</b>	<b>8</b>
2.1 Morphology and Chemical Structure	8
2.2 Soot Formation Chemistry	8
2.2.1 Formation of benzene	9
2.2.1.1 Acetylene	10
2.2.1.2 Propargyl radical	10
2.3 Summary	11
<b>Chapter 3: Combustion in Diesel Engines</b>	<b>12</b>
3.1 Delay period	12
3.2 Period of Premixed Combustion	13
3.3 Period of Mixing Controlled Combustion	13
3.4 Summary	14
<b>Chapter 4: Senkin Analysis</b>	<b>15</b>
4.1 Formulation	15
4.2 Results and Discussion	16
4.3 Conclusions	44
<b>Chapter 5: PSR Analysis</b>	<b>45</b>
5.1 Formulation	45
5.2 Results and Discussion	47
5.3 Conclusions	56
<b>Chapter 6. Conclusions</b>	<b>57</b>
6.1 Conclusions from the Senkin Simulations	57
6.2 Conclusion from the PSR Simulations	59
<b>Chapter 7: Recommendations for Future Work</b>	<b>60</b>
7.1 Use of an additional program	60
7.2 Description of KIVA3	61
7.3 Formulation of KIVA3	61
<b>REFERENCES</b>	<b>63</b>

<i>APPENDIX A: Senkin input file for the expansion stroke. (Case A)</i>	<u>68</u>
<i>APPENDIX B: Senkin input file for the expansion stroke. (Case B)</i>	<u>69</u>
<i>APPENDIX C: Reaction Scheme for Ozone</i>	<u>70</u>
<i>APPENDIX D: Volume as a function of time (Senkin Simulation)</i>	<u>71</u>
<i>VITA</i>	<u>73</u>

## List of Figures

Figure 1.1: The Reaction Pathways for RO <sub>2</sub> Radicals	3
Figure 1.2: Diagram of simulated strokes used in the computational analyses.	5
Figure 4.1: The concentration of H <sub>2</sub> O and H <sub>2</sub> as a function of position in the expansion stroke at any of the three speeds and eight levels of ozone. Trends shown start at top dead center and end shortly after ignition.	16
Figure 4.2: The temperature of the no ozone case and concentration of CO <sub>2</sub> as a function of position in the expansion stroke at a speed of 1500 rpm and ozone levels of 0 PPM and 1000 PPM. Trends shown start at top dead center and end shortly after ignition.	17
Figure 4.3: The temperature of the no ozone case and concentration of CO as a function of position in the expansion stroke at a speed of 1500 rpm and ozone levels of 0 PPM and 1000 PPM. Trends shown start at top dead center and end shortly after ignition.	18
Figure 4.4: The temperature and concentration of O <sub>3</sub> as a function of position in the expansion stroke at any of three speeds and eight ozone levels. Trends shown start at bottom dead center and end shortly after first time step.	19
Figure 4.5: The temperature and concentration of O <sub>3</sub> as a function of position in the compression stroke at 1500 and 2500 RPM. Ozone level is 1000 PPM. Trends shown start shortly before the decomposition of ozone and end at the top dead center.	20
Figure 4.6: The temperature of the no ozone case and concentration of O as a function of position in the expansion stroke at an engine speed of 1500 rpm. Ozone level is 1000 PPM and all injection times are displayed. Trends shown start at top dead center and end shortly after ignition.	21
Figure 4.7: The temperature of the no ozone case and concentration of O as a function of position in the expansion stroke at an engine speed of 1500 rpm. Ozone level is 1000 PPM and all injection times are displayed. Trends shown start at shortly after ignition and end bottom dead center	21
Figure 4.8: The temperature of the no ozone case and concentration of H as a function of the position of the expansion stroke at engine speeds of 1500 and 2500 rpm for any ozone level and injection time. Trends shown start at top dead center and end shortly after ignition.	22
Figure 4.9: The temperature of the no ozone case and concentration of OH as a function of position in the expansion stroke at an engine speed of 1500 rpm. Ozone level is 25 PPM and all injection times are displayed. Trends shown start at top dead center and end shortly after ignition.	24
Figure 4.10 The concentration of OH as a function of position in the expansion stroke at an engine speed of 1500 rpm. Ozone level is 25 PPM and all injection times are displayed. Trends shown start shortly after ignition and end at bottom dead center.	24
Figure 4.11: The temperature of the no ozone case and concentration of OH as a function of position in the expansion stroke at an engine speed of 2500 rpm. Ozone level is 25 PPM and	

all injection times are displayed. Trends shown start at top dead center and end shortly after ignition.	25
Figure 4.12: The concentration of OH as a function of position in the expansion stroke at an engine speed of 2500 rpm. Ozone level is 25 PPM and all injection times are displayed. Trends shown start shortly after ignition and end at bottom dead center.	25
Figure 4.13: The temperature of the no ozone case and concentration of OH as a function of position in the expansion stroke at an engine speed of 1500 rpm. Ozone level is 100 PPM and all injection times are displayed. Trends shown start at top dead center and end shortly after ignition.	26
Figure 4.14: The concentration of OH as a function of position in the expansion stroke at an engine speed of 1500 rpm. Ozone level is 100 PPM and all injection times are displayed. Trends shown start at shortly after ignition and end bottom dead center	26
Figure 4.15: The temperature of the no ozone case and concentration of OH as a function of position in the expansion stroke at an engine speed of 2500 rpm. Ozone level is 100 PPM and all injection times are displayed. Trends shown start at top dead center and end shortly after ignition.	27
Figure 4.16 The concentration of OH as a function of position in the expansion stroke at an engine speed of 2500 rpm. Ozone level is 100 PPM and all injection times are displayed. Trends shown start at shortly after ignition and end bottom dead center	27
Figure 4.17: The temperature of the no ozone case and concentration of OH as a function of position in the expansion stroke at an engine speed of 1500 rpm. Ozone level is 1000 PPM and all injection time are displayed. Trends shown start at top dead center and end shortly after ignition.	28
Figure 4.18: The concentration of OH as a function of position in the expansion stroke at an engine speed of 1500 rpm. Ozone level is 1000 PPM and all injection times are displayed. Trends shown start at shortly after ignition and end bottom dead center	28
Figure 4.19: The temperature of the no ozone case and concentration of OH as a function of position in the expansion stroke at an engine speed of 2500 rpm. Ozone level is 1000 PPM and all injection times are displayed. Trends shown start at top dead center and end shortly after ignition.	29
Figure 4.20: The concentration of OH as a function of position in the expansion stroke at an engine speed of 2500 rpm. Ozone level is 1000 PPM and all injection times are displayed. Trends shown start at shortly after ignition and end bottom dead center.	29
Figure 4.21: The temperature of the no ozone case and concentration of $C_2H_2$ as a function of position in the expansion stroke at an engine speed of 1500 rpm. Ozone level is 25 PPM and all injection times are displayed. Trends shown start at top dead center and end shortly after ignition.	31
Figure 4.22: The concentration of $C_2H_2$ as a function of position in the expansion stroke at an engine speed of 1500 rpm. Ozone level is 25 PPM and all injection times are displayed. Trends shown start shortly after ignition and end at bottom dead center.	31
Figure 4.23: The temperature of the no ozone case and concentration of $C_2H_2$ as a function of position in the expansion stroke at an engine speed of 2500 rpm. Ozone level is 25 PPM and	

all injection times are displayed. Trends shown start at top dead center and end shortly after ignition.	32
Figure 4.24: The concentration of $C_2H_2$ as a function of position in the expansion stroke at an engine speed of 2500 rpm. Ozone level is 25 PPM and all injection times are displayed. Trends shown start shortly after ignition and end at bottom dead center.	32
Figure 4.25: The temperature of the no ozone case and concentration of $C_2H_2$ as a function of position in the expansion stroke at an engine speed of 1500 rpm. Ozone level is 100 PPM and all injection times are displayed. Trends shown start at top dead center and end shortly after ignition.	33
Figure 4.26: The concentration of $C_2H_2$ as a function of position in the expansion stroke at an engine speed of 1500 rpm. Ozone level is 100 PPM and all injection times are displayed. Trends shown start shortly after ignition and end at bottom dead center.	33
Figure 4.27: The temperature of the no ozone case and concentration of $C_2H_2$ as a function of position in the expansion stroke at an engine speed of 2500 rpm. Ozone level is 100 PPM and all injection times are displayed. Trends shown start at top dead center and end shortly after ignition.	34
Figure 4.28: The concentration of $C_2H_2$ as a function of position in the expansion stroke at an engine speed of 2500 rpm. Ozone level is 100 PPM and all injection times are displayed. Trends shown start shortly after ignition and end at bottom dead center.	34
Figure 4.29: The temperature of the no ozone case and concentration of $C_2H_2$ as a function of position in the expansion stroke at an engine speed of 1500 rpm. Ozone level is 1000 PPM and all injection times are displayed. Trends shown start at top dead center and end shortly after ignition.	35
Figure 4.30: The concentration of $C_2H_2$ as a function of position in the expansion stroke at an engine speed of 1500 rpm. Ozone level is 1000 PPM and all injection times are displayed. Trends shown start shortly after ignition and end at bottom dead center.	35
Figure 4.31: The temperature of the no ozone case and concentration of $C_2H_2$ as a function of position in the expansion stroke at an engine speed of 2500 rpm. Ozone level is 1000 PPM and all injection times are displayed. Trends shown start at top dead center and end shortly after ignition.	36
Figure 4.32: The concentration of $C_2H_2$ as a function of position in the expansion stroke at an engine speed of 2500 rpm. Ozone level is 1000 PPM and all injection times are displayed. Trends shown start shortly after ignition and end at bottom dead center.	36
Figure 4.33: The temperature of the no ozone case and concentration of $C_3H_3$ as a function of position in the expansion stroke at an engine speed of 1500 rpm. Ozone level injected 25 PPM and all injection times are displayed. Trends shown start at top dead center and end shortly after ignition.	38
Figure 4.34: The concentration of $C_3H_3$ as a function of position in the expansion stroke at an engine speed of 2500 rpm. Ozone level injected 25 PPM and all injection times are displayed. Trends shown start at top dead center and end shortly after ignition	38
Figure 4.35: The temperature of the no ozone case and concentration of $C_3H_3$ as a function of position in the expansion stroke at an engine speed of 2500 rpm. Ozone level injected 25	

PPM and all injection times are displayed. Trends shown start at top dead center and end shortly after ignition.	39
Figure 4.36: The concentration of $C_3H_3$ as a function of position in the expansion stroke at an engine speed of 2500 rpm. Ozone level injected 25 PPM and all injection times are displayed. Trends shown start shortly after ignition and end at bottom dead center.	39
Figure 4.37: The temperature of the no ozone case and concentration of $C_3H_3$ as a function of position in the expansion stroke at an engine speed of 1500 rpm. Ozone level injected 100 PPM and all injection times are displayed. Trends shown start at top dead center and end shortly after ignition.	40
Figure 4.38: The concentration of $C_3H_3$ as a function of position in the expansion stroke at an engine speed of 1500 rpm. Ozone level injected 100 PPM and all injection times are displayed. Trends shown start shortly after ignition and end at bottom dead center.	40
Figure 4.39: The temperature of the no ozone case and concentration of $C_3H_3$ as a function of position in the expansion stroke at an engine speed of 2500 rpm. Ozone level injected 100 PPM and all injection times are displayed. Trends shown start at top dead center and end shortly after ignition.	41
Figure 4.40: The concentration of $C_3H_3$ as a function of position in the expansion stroke at an engine speed of 2500 rpm. Ozone level injected 100 PPM and all injection times are displayed. Trends shown start shortly after ignition and end at bottom dead center.	41
Figure 4.41: The temperature of the no ozone case and concentration of $C_3H_3$ as a function of position in the expansion stroke at an engine speed of 1500 rpm. Ozone level injected 1000 PPM and all injection times are displayed. Trends shown start at top dead center and end shortly after ignition.	42
Figure 4.42: The concentration of $C_3H_3$ as a function of position in the expansion stroke at an engine speed of 1500 rpm. Ozone level injected 1000 PPM and all injection times are displayed. Trends shown start shortly after ignition and end at bottom dead center.	42
Figure 4.43: The temperature of the no ozone case and concentration of $C_3H_3$ as a function of position in the expansion stroke at an engine speed of 2500 rpm. Ozone level injected 1000 PPM and all injection times are displayed. Trends shown start at top dead center and end shortly after ignition.	43
Figure 4.44: The concentration of $C_3H_3$ as a function of position in the expansion stroke at an engine speed of 2500 rpm. Ozone level injected 1000 PPM and all injection times are displayed. Trends shown start shortly after ignition and end at bottom dead center.	43
Figure 5.1: The concentration of $H_2O$ as a function of the initial concentration of ozone at engine speeds of 1500 and 2500 rpm. The four ozone levels displayed are 0, 25, 100, and 1000 ppm.	47
Figure 5.2: The concentration of $H_2$ as a function of the initial concentration of ozone at engine speeds of 1500 and 2500 rpm. The four ozone levels displayed are 0, 25, 100, and 1000 ppm.	47
Figure 5.3: The concentration of $CO_2$ as a function of the initial concentration of ozone at engine speeds of 1500 and 2500 rpm. The four ozone levels displayed are 0, 25, 100, and 1000 ppm.	48

Figure 5.4: The concentration of CO as a function of the initial concentration of ozone at engine speeds of 1500 and 2500 rpm. The four ozone levels displayed are 0, 25, 100, and 1000 ppm.	49
Figure 5.5: The concentration of O <sub>3</sub> as a function of the initial concentration of ozone at engine speeds of 1500 and 2500 rpm. The four ozone levels displayed are 0, 25, 100, and 1000 ppm.	50
Figure 5.6: The concentration of O <sub>2</sub> as a function of the initial concentration of ozone at engine speeds of 1500 and 2500 rpm. The four ozone levels displayed are 0, 25, 100, and 1000 ppm.	51
Figure 5.7: The concentration of O as a function of the initial concentration of ozone at engine speeds of 1500 and 2500 rpm. The four ozone levels displayed are 0, 25, 100, and 1000 ppm.	51
Figure 5.8: The concentration of H as a function of the initial concentration of ozone at engine speeds of 1500 and 2500 rpm. The four ozone levels displayed are 0, 25, 100, and 1000 ppm.	52
Figure 5.9: The concentration of OH as a function of the initial concentration of ozone at engine speeds of 1500 and 2500 rpm. The four ozone levels displayed are 0, 25, 100, and 1000 ppm.	53
Figure 5.10: The concentration of C <sub>2</sub> H <sub>2</sub> as a function of the initial concentration of ozone at engine speeds of 1500 and 2500 rpm. The four ozone levels displayed are 0, 25, 100, and 1000 ppm.	54
Figure 5.11: The concentration of C <sub>3</sub> H <sub>3</sub> as a function of the initial concentration of ozone at engine speeds of 1500 and 2500 rpm. The four ozone levels displayed are 0, 25, 100, and 1000 ppm.	55

## Chapter 1: Introduction

Government fuel economy standards have prompted automobile manufacturers to seek new means to increase fleet average fuel mileage (Bechtold, et al., 1984). One popular modification is to replace the gasoline engine with a more efficient diesel engine. The diesel engine has up to 25% better efficiency in comparison with the gasoline engine (Schindler and Hentschel, 1992). Although this modification is fuel efficient, the tradeoff is the lack of an effective way to control the diesel engine emissions. In gasoline engines, the preferred method for emission control is a three-way catalyst which removes nitrogen oxides, carbon monoxide, and unburned hydrocarbons (UHC). Unfortunately, this method can not be implemented in the diesel engine due to the particulates in the exhaust gases.

The exhaust gases from diesel engines have a detrimental effect on the environment because they contribute to air pollution. This problem stems from the fact that diesel engines have particulate emissions that are ten times higher than non-catalyst gasoline engines. Numerical investigations show that soot emissions reach a level of approximately 1g / mile depending on the engine type and the driving conditions (Zierok, 1981). The quantity of soot is also dependent on the combustion conditions and fuel properties.

Due to the increased use of diesel engines, the Environmental Protection Agency (EPA) has started setting standards to decrease toxic exhaust emissions. In 1987, the EPA particulate certification standard for light duty diesel engine vehicles was 0.2 g / mile. However, the Clean Air Act Amendment of 1990 [ 203(g) (2)] prescribed particulate emission standards for light duty diesel vehicles and trucks of 0.08 g / mile and 0.1 g / mile respectively, which will reach full implementation by the end of 1997 (Docekal, et al., 1992). With the EPA lowering the standards of toxic exhaust emissions and the increasing concern of the environment, new technology is needed to reduce the formation and growth of soot in diesel engines.

### 1.1 Previous Work

In June 1993, an inventor found that supplying ozone through the intake manifold improved the performance of his gasoline fueled car. As a result of these findings, he approached the Science Applications International Corporation (SAIC) who then following his lead and investigated his discoveries further. SAIC conducted experimental tests on a 1993 Lincoln Town Car to determine the effects of ozone addition on the exhaust emissions of gasoline engines. The testing results supplied convincing evidence of reduced levels of  $\text{NO}_x$  and UHC in the exhaust gases. However, SAIC did not have enough resources to perform an extensive parametric study. It was obvious a more detailed analysis was needed to determine the chemical potential of ozone

to reduce internal combustion engine emissions. An analysis was performed by Balakrishnan (1994); details of the examination are summarized in the next section.

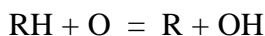
### 1.1.1 Chemical Kinetic Analysis

The effect of ozone on oxidation rates of hydrocarbons has been studied extensively with the earliest investigation done by Otto in 1898 (Otto, 1898). In conclusion of these early studies, it was found that the reaction rates of hydrocarbons were greater than the reaction rates of ozone. This evidence led researchers such as Otto to believe that ozone directly attacked the C-H bonds in hydrocarbons.

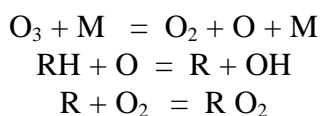
At high temperatures (above 900K), initiation occurs by the molecular decomposition of the fuel molecules in the reactions listed below:



At low temperatures, however, (below 900 K), initiation occurs through the oxidation of hydrocarbons:



with reaction constants of  $1.67 \times 10^{13} \exp(-7850 / RT)$ ,  $1.4 \times 10^{13} \exp(-5200 / RT)$  and  $1.00 \times 10^{13} \exp(-3280 / RT) \text{ cm}^3 \text{ mole}^{-1} \text{ s}^{-1}$  for every primary, secondary and tertiary C-H bonds, respectively. The alkyl radicals generated from this step readily adds on molecular oxygen to form  $RO_2$  (Benson, 1965). The initiation step is important because ozone starts to decompose at approximately 800K. When ozone is added into the air intake of a spark ignited engine, the fuel can be anticipated to undergo the following reactions (Westbrook et al., 1988).



The  $RO_2$  radicals are extremely unstable at high temperatures (above 800K (Warnatz, 1981; Benson, 1981)) and high pressures, and rapidly decompose to form OH and other active radicals by the reactions shown in Figure 1 (Benson, 1981; Pollard, 1977).



ozone has on the oxidation of hydrocarbons. Two programs were used to aid in the understanding of the combustion pollutant formation; Senkin and PSR.

Senkin is a Fortran program developed by Sandia National Laboratories. This program computes the time evolution of the homogenous premixed reacting gas mixture in a closed system. This program is able to predict species and temperature histories. In this thesis, research was done modeling the diesel engine as an adiabatic system with volume as a specified function of time; and only the compression and expansion strokes in the four stroke diesel cycle was modeled.

PSR is a Fortran program that models perfectly stirred reactors which was also developed by Sandia National Laboratories. This code predicts the steady-state temperature and species composition in a perfectly stirred reactor. The reactors are thermally insulated with inlet and outlet ducts similar to a control volume. The flow in the reactor is characterized by the nominal residence time; and only the expansion stroke in the four stroke diesel cycle was modeled. The reacting gas mixture was homogenous and premixed.

When modeling the combustion processes of a diesel engine, there are numerous reactions to analyze. With this in mind, the computational analysis can be very complex requiring extensive computational resources. Therefore, irrelevant reactions were eliminated that did not play a role in this research. This reduced chemical kinetic scheme maintains all essential features but with fewer species and reaction steps which reduces computational time.

In this simulation, there were approximately four hundred species and close to two thousand reactions involved in the chemical mechanism used. Therefore, a decision of what species to analyze became very relevant. Based on the knowledge obtained from extensive research, eleven species were chosen. The analyzed species are the following: carbon dioxide ( $\text{CO}_2$ ), water ( $\text{H}_2\text{O}$ ), carbon monoxide ( $\text{CO}$ ), monatomic hydrogen ( $\text{H}$ ), diatomic hydrogen ( $\text{H}_2$ ), ozone ( $\text{O}_3$ ), monatomic oxygen ( $\text{O}$ ), diatomic ( $\text{O}_2$ ), hydroxyl ( $\text{OH}$ ), acetylene ( $\text{C}_2\text{H}_2$ ), and propargyl radical ( $\text{C}_3\text{H}_3$ ). The net chemical production rate of each species is a function of temperature since the forward reaction rate was in the Arrhenius form in both analyses.

In this investigation, the combusting fuel used was hexane ( $\text{C}_6\text{H}_{14}$ ) instead of an actual diesel fuel complex. Hexane was chosen as the combusting fuel because the diesel fuel mechanism contained numerous complex reactions which would cause the simulations to run for a long time. Past work found that in the absence of  $\text{C}_{7+}$  alkane data that possible concentrations were estimated using hexane (Hucknall, 1985).

## 1.2 Formulation of Initial Conditions

The diesel cycle involves four strokes: intake, compression, expansion and exhaust. In both models, the intake and exhaust strokes were not simulated but, models were turbocharged before the compression stroke as seen in the diagram below.

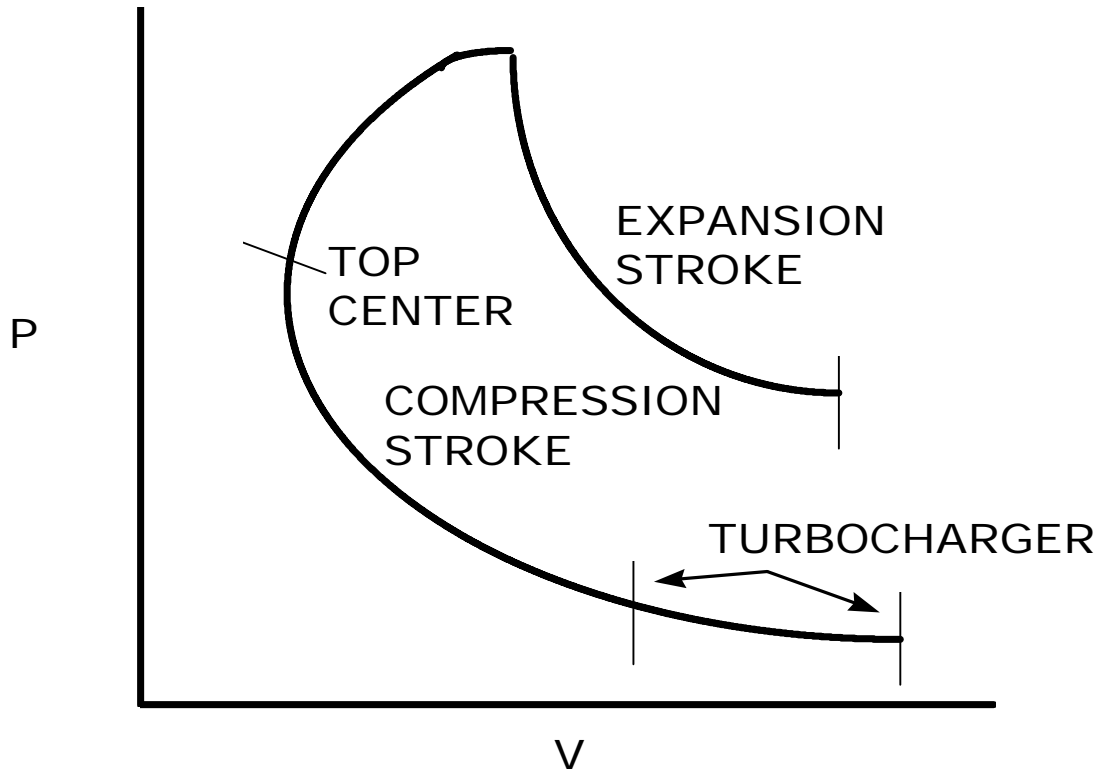


Figure 1.2: Diagram of simulated strokes used in the computational analyses.

Since the models were initially turbocharged, several assumptions were made to calculate the initial pressure and temperature conditions of the compression stroke. The compressor efficiency ( $\eta_c$ ) was assumed to be equal to .70 and  $C_p$  was constant in the equation 1.1 (See below)

$$h_c = \frac{C_p \cdot (T_{ib} - T_0)}{C_p \cdot (T_1 - T_0)} \quad (E1.1)$$

where  $T_0$  = ambient temperature,  $T_1$  = actual temperature after compression, and  $T_{ib}$  = isentropic temperature after compression. The compressor efficiency equation was used in conjunction with the polytropic relationship (E1.2) to calculate the two unknown temperatures,  $T_1$  and  $T_{ib}$ .

$$\frac{T_{ib}}{T_o} = \left( \frac{P_1}{P_o} \right)^{\frac{k-1}{k}} \quad (E1.2)$$

In polytropic relationship,  $P_0$  = ambient pressure and the polytropic constant,  $k = 1.4$ . The intake manifold pressures for each speed were found from dyno testing of a Cummins 4BT3.9 engine which are listed below.

<u>Speed (RPM)</u>	<u>Intake Manifold Pressure (in Hg)</u>
1500	20.0
2000	26.6
2500	34.1

Depending on the engine speed used in the simulation, the intake manifold pressure,  $P_i$ , was used to find  $P_1$  as seen in the equation 1.3.

$$P_1 = (P_i + P_o) \quad (E1.3)$$

The compressor efficiency equation, polytropic relationship, and the above pressure equation were used to calculate the initial conditions of the compression stroke. The displaced piston volume was 980 ml which was calculated when the bore diameter was equal to 102 mm and the stroke was equal to 120 mm. The compression ratio was 17.5 to 1 and the piston movement in the simulations was linear instead of sinusoidal.

### 1.3 Computational considerations

The composition of the diesel engine exhaust emissions is extremely complex and is influenced by engine type, speed and load, driving patterns, air-to-fuel ratio, operation temperature, fuel composition, and oil consumption (Docekal, et al, 1992). In this thesis, the numerical simulations are functions of ozone concentration, speed of the diesel engine, inlet temperature and pressure, and the equivalence ratio. Each variable is described below in more detail.

- Ozone Concentration. Eight levels of ozone concentration ranging from 0 PPM to 1000 PPM were considered. The actual levels are the following: 0, 25, 50, 100, 250, 500, 750, 1000 PPM.
- Speed of the engine. Simulations modeled the diesel engine at three speeds: 1500, 2000, and 2500 rpm. 1500 rpm is the low engine speed; 2000 rpm is the idle engine speed; and 2500 rpm is the high engine speed.
- Inlet temperature and pressure. The inlet temperature and pressure were functions of the engine speed and were calculated using the polytropic relationship, compressor efficiency and intake manifold pressure.
- Equivalence Ratio. The equivalence ratio was 0.6. To avoid the formation of soot during combustion the mixture should be in the area of  $0.6 < \phi < 0.8$  (Schindler and Hentshel, 1992).

### 1.4 Motivation

In today's environmentally conscious society, emission control has become more of a necessity than a desire. The increasing use of diesel engines has sparked numerous studies and experiments on how to control soot, a toxic by-product of combustion. SAIC preliminary testing has found evidence of a possible solution in reducing levels of exhaust fumes by adding ozone. The scope of this thesis was to determine the effect ozone has on diesel soot precursors.

## Chapter 2: Soot

Soot is a fine dispersion of black carbon particles in a vapor carrier. The main source of soot is from incomplete hydrocarbon combustion. Soot particles form, grow, and are oxidized as a result of complex chemical reactions that occurs during combustion. These reactions can generate particles within milliseconds that contain an abundance of carbon atoms. Some of these reactions decrease the black carbon particle mass, while others react simultaneously on the same carbon particles. Therefore, the reactions taking place have unverified chemical routes.

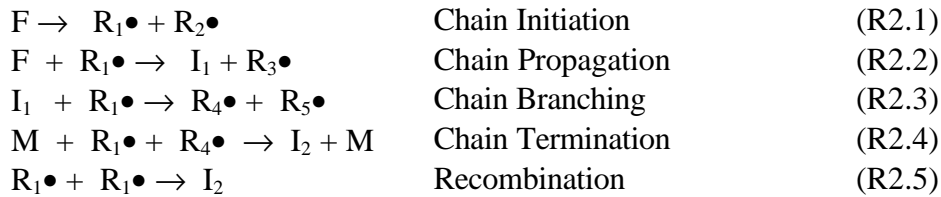
### 2.1 Morphology and Chemical Structure

Particles characteristics from the pyrolysis of a hydrocarbon fuel molecule depends on the degree of formation. In the early stages of formation, the soot particles are fuel specific and have a spherical shape with a diameter range of three to twelve nanometers. However, the later stages of formation generate particles having a chain-like appearance. The chain links have numerous clusters of spherical particles with a diameter range of two to thirty-five nanometers. Research shows that only the early accumulation of particles are affected by the fuel type, but not the ultimate chemical character of soot particles. (Saito, et al., 1991).

The chemical makeup of soot includes an abundance of carbon in addition to hydrogen, oxygen, and a minute amount of nitrogen. Although, the actual chemical composition is contingent on the fuel type and how the soot particles grow and mature. The composition of soot is attributed to the reactive surface of the particles which readily adsorbs gas phase species, enabling the formation of surface complexes with carbon (Glassman, 1988). The highly stable polycyclic aromatic hydrocarbons (PAH) are adsorbed on the soot and maintain their structure as the particle is emitted from the flame (Lee, Novotony, Bartle, 1976). Younger particles have a much higher hydrogen content and possess a larger number of reactive radical sites (Haynes and Wagner, 1983).

### 2.2 Soot Formation Chemistry

During the decomposition of a hydrocarbon fuel in a combustion process, a series of chain reactions take place. The first reaction is chain initiation where the fuel dissociates to generate free radicals. These flame radicals take part in a list of chain reactions which lead to molecular growth. The following classes of reactions are important in molecular growth:



where F = fuel,  $R_n\bullet$  = radical,  $I_n$  = intermediate, M = third body, and  $k_n$  = reaction rate constant ( $n = 1,2,3\dots$ ). These general reactions listed above outline the chemical production of soot.

The evolution of soot has five stages which are: fuel pyrolysis, formation of particle nuclei, particle growth, agglomeration or coagulation, and oxidation. As seen in reaction 2.1, the fuel dissociates and forms flame radicals. The complex chemical reactions taking place have unverified chemical routes but regardless of route there is a common mechanism of soot evolution. The common mechanism includes the rate of formation of the first and second aromatic rings from pyrolysis of fuel, which is the rate controlling step in soot formation (Aftel, 1993).

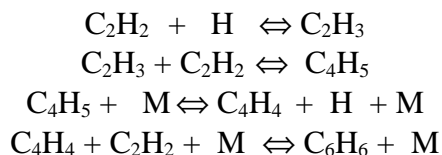
### 2.2.1 Formation of benzene

The formation of benzene from aliphatics can occur in at least two ways. The first and most common way is the addition of  $C_2$  species to  $C_4$  species. The other way is the addition of  $C_3$  species to  $C_3$  species. The formation of aromatics depends on the fuel type and the experimental configuration. The experimental configuration involves the time and temperature characteristics of the combustion process and whether a premixed, nonpremixed (diffusion) flames, or a combination of two flame types is used; while with the fuel type, there are numerous possibilities.

In a diffusion flame, benzene and soot form before the main reaction zone, hence making the fuel structure effects more pronounced. The soot formation and oxidation do not occur concurrently. The soot forms on the fuel side where there is essentially no competitive oxidation. So, the formation of soot becomes a direct function of the temperature. However in a premixed flame, the fuel structure effects are not strong because the parent fuel decomposes to acetylene ( $C_2H_2$ ) in the main reaction zone prior to soot inception. The soot formation and oxidation occurs simultaneously. Increases in flame temperature causes a decrease in soot formation, since oxidative reactions become faster than pyrolytic reactions at higher temperature, and oxidation dominates( Aftel, 1993).

### 2.2.1.1 Acetylene

Normally when a hydrocarbon fuel decomposes, it breaks down and generates acetylene ( $C_2H_2$ ).  $C_2H_2$  is the most dominant intermediate formed after a chain propagating reaction, as seen above in reaction 2.2. This  $C_2H_2$  then bonds with H and other  $C_2H_2$  groups until a benzene ring is formed. Now, the formation of benzene is not an immediate result, it usually involves several steps, as listed below.



The ring forming process begins with  $C_2H_2$ , which grows by an addition of hydrogen forming the vinyl radical ( $C_2H_3$ ). The vinyl radical is then added to another acetylene which results in the formation of the butadienyl radical ( $C_4H_5$ ). This process continues when  $C_4H_5$  loses a H molecule and produces vinylacetylene ( $C_4H_4$ ); and then the subjoining of  $C_2H_2$  forms the final result, benzene ( $C_6H_6$ ). M, which is present in the third and fourth reactions, is a third body. The third body adsorbs or creates the necessary energy needed for these reactions to take place. Now, the path of the formation of the first aromatic ring described here is not the only route for generating benzene. As mentioned earlier, the actual path is unconfirmed because there are a number of different routes that could be taken; this example is just one of many.

### 2.2.1.2 Propargyl radical

Another pathway for the evolution of the initial aromatic ring, is the subjoining of two  $C_3$  species. Research shows that when certain fuel types are used, there were high concentrations of  $C_3$  species, but low concentrations of  $C_2$  species (Sidebotham and Glassman, 1992). Therefore in those cases, the  $C_3$  species was the dominant intermediate in the generation of the initial aromatic ring and was represented by the propargyl radical ( $C_3H_3$ ).  $C_3H_3$  is formed from the decomposition of the parent fuel and bonds with another  $C_3H_3$  group until benzene is formed (See reaction below).



Since  $C_3$  species are highly reactive, more soot is formed through the  $C_3$  species path. (Miller, 1992 and Sidebotham, 1992).

## 2.3 Summary

$C_2$  and  $C_3$  species are seen as prominent precursors of soot.  $C_3H_3$  has no weak bonds and its addition tends to be highly reversible (Miller and Melius, 1992). However,  $C_2H_2$  is likely to be the dominant soot growth species because of its high concentration.

Soot inception is observed only when local temperature exceeds a critical value in a region far from the oxidation zone. But, the fuel structure plays a small role in determining if soot inception occurs (Sidebotham and Glassman, 1992). As stated throughout this chapter, the precise path of the first benzene structure is not authenticated; therefore in the chemical analysis of the effect of ozone on diesel soot precursors, the concentrations of acetylene and the propargyl radical have both been investigated.

## Chapter 3: Combustion in Diesel Engines

The diesel engine is a popular alternative to the spark-ignition engine because it is 25% more efficient. However, this increased efficiency comes with a tradeoff which is the environmentally hazardous soot emissions. These soot emissions are byproducts of incomplete combustion that takes place in the diesel engine.

Combustion in a diesel engine can be described in three stages: the delay period, the period of premixed combustion, and the period of mixing-controlled combustion. The phase of combustion affects the droplets concentration because the heterogeneous mixture burned during the combustion process is constantly changing. The droplet concentration involves fuel, air, or combination of the two; therefore, when a flame is generated during these three phases, it possesses the characteristics of both a premixed and nonpremixed (diffusion) flame.

### 3.1 Delay period

The delay period, which is sometimes called the ignition lag, is the first stage of combustion. This period is composed of preliminary reactions that occur prior to the appearance of a flame, and begins with the injection of the fuel spray into the combustion chamber. The fuel enters the chamber before the cycle's top dead center position. As the injected spray enters the combustion cell, it slowly "bores a hole" in the air, while fuel particles are stripped away, some being vaporized (Obert, 1973).

After the injection of the fuel, the fuel droplets go through a series of phases. Initially, each fuel droplet is surrounded by vapor immediately after entering the combustion chamber. In the vapor surrounding the droplet surface, chemical reactions start simultaneously with the injection of each fuel drop in the cylinder. These chemical reactions are either cool-flame reactions on the verge of autoigniting or cracking reactions on the verge of forming luminescent carbon particles. The fuel volatility has little effect on the delay period because of these chemical reactions.

The phase of ignition lag period is controlled by properties of the combustion chamber. The temperature, fuel composition, and impingement of the spray on the hot surfaces has a pronounced effect on the chemical reactions during the ignition lag period. The fuel-air ratio modifies the time between the completion of the compression process and the appearance of the flame. There is a complete range of fuel-air ratios; the range includes a fuel-air ratio of zero, which is the no fuel case, to a fuel-air ratio of infinity, which is the no air case. The combustion rate of the droplets are limited by their evaporation rate; and the burning rate decreases as the fraction of oxygen in the surrounding air decreases. Although, the pressure greatly influenced the ignition and combustion rate, it has a small effect on the ignition lag period.

### **3.2 Period of Premixed Combustion**

The period of premixed combustion is the second stage of combustion. During this stage, the combustion process shows the characteristics of a premixed flame. The period begins with a visible flame at one or more locations that turbulently spreads with growing luminosity. The exact moment that the flame is visible is defined as ignition, and takes place as a result of a volumetric heat release in the engine. In the diesel engine, ignition is called autoignition because it initiates the combustion process by design unlike the spark- ignited engine. Autoignition is identified by a rapid pressure rise and high rate of energy release which leads to the sound of engine knock.

The flame usually appears while the fuel and air mixture is nonuniform, and the fuel is still a liquid. The low luminosity characterizes the presence of a premixed flame. The initial spreading of the nonluminous and luminous flame arises from autoignition and flame propagation occurring simultaneously in the spray envelope (Obert, 1973). Since regions of premixed flames are probably hotter (and “older”) than regions where liquid droplets are present, the knock reaction may be propagated mainly in the low luminosity stage of the flame (Austin, 1961 and Alcock, 1963).

During this stage, the evaporated fuel that has mixed with the air during the delay period is burned. Therefore, the burning rate of the second stage is related to the delay period and the fuel injection rate. Since the fuel injection rate is directly proportional to the engine speed, the amount of the fuel injected during the delay period is also proportional to the engine speed. The burning rate and pressure rise during this stage increases as the delay period increases which is a direct result of the mixing time and the greater fuel quantity. However, the delay only has a strong influence on the second phase when the delay period is shorter than injection period (Taylor, 1968).

### **3.3 Period of Mixing Controlled Combustion**

The period of mixing controlled combustion is the third stage of combustion. This period has characteristics that are similar to a diffusion flame and only involves fuel that has not found the necessary oxygen during the period of premixed combustion. The flame seen during this stage has a high luminosity which characterizes the presence of the diffusion flame. The flame spreads rapidly as the turbulent, heterogeneous flame propagates with a decreasing energy rate.

The third phase of combustion is the time when pressure is at its maximum and where the combustion process is virtually complete. The combustion rate is limited by only the mixing process. This in turn is controlled by the ratio of oxygen to unburned fuel and by the degree to which the two are distributed and mixed at the end of the second period (Taylor, 1968). Even in this stage, small autoigniting regions must be present which is probably the source of

microturbulence (Obert, 1973). This microturbulence allow air to mix with soot clouds that appears after the top dead center position.

### **3.4 Summary**

The diesel engine cycle involves numerous chemical reactions. All of these reactions were explicated from the descriptions of the three combustion phases. It was found that the conditions of the three combustion phases worked together interdependently. Properties, like temperature, pressure, fuel type, fuel volatility, speed, fuel-air ratio, and turbulence, were all contributing factors to the environment of the combustion chamber. Some chemical reactions take place due to the high temperature and pressure. In the second and third stages of combustion, the burning rates are nearly proportional to the speed. The ignition and the combustion rate are both influenced by the timing and rate of fuel injection, the pressure and temperature of the chamber, and the turbulence of compressed air. The delay time increases with a decreasing fuel-air ratio because of the reduction of the wall temperature. In the computational model of a compression-ignited engine used in this thesis, the engine speed was the only contributing factor used to investigate the effect of ozone on diesel soot precursors.

## Chapter 4: Senkin Analysis

Senkin is a Fortran computer program that computes the time evolution of a homogenous premixed gas mixture in a closed system. This program models an idealistic system with zero dimension. The program can be applied for five problem types but in this analysis only one was used. The problem description for this analysis is an adiabatic system where the volume is a specified function of time. The output generated from this program predicts the time-dependent chemical kinetic behavior of the specified system type. This program is run concomitantly with CHEMKIN which is used to evaluate the chemical reaction mechanism.

In a compression ignition (CI) engine, a heterogeneous mixture of air and fuel is burned during the diesel cycle. This mixture is influenced by turbulence and friction effects in a non adiabatic system; and the volume is a function of time which is determined by the speed of engine. With that knowledge, Senkin seems to be an ineffective method of modeling what happens in CI engine. Although Senkin does not model a system with a heterogeneous mixture of gases that is strongly influenced by turbulence and friction, it can still be used to understand combustion pollutant formation.

### 4.1 Formulation

Because of the limitations of the Senkin program, several modifications were made to simulate a realistic analogous archetype of a CI engine. Hexane ( $C_6H_{14}$ ) was the combusting fuel used instead of an actual diesel fuel complex. The actual diesel cycle was a four stroke cycle but Senkin only modeled two strokes, compression and expansion. The intake and exhaust strokes were neglected since the primary focus of this simulation was chemical kinetics.

The initial engine temperature and pressure of the compression stroke were calculated solving three equations simultaneously which were: the polytropic relationship, the compressor efficiency equation, and the intake manifold pressure equation. The initial temperature and pressure of the expansion stroke was assumed to be the final temperature and pressure of the compression stroke. Three speeds, 1500, 2000, and 2500 rpm, were utilized and there were eight different ozone levels that ranged from 0 to 1000 PPM. Ozone was injected at two different times.

The first time (known as CASE A here after) was at the beginning of the compression stroke with air; where this gas mixture was compressed. At the beginning of the expansion stroke, fuel was injected for autoignition. At the second injection time (known as CASE B), ozone was injected with the fuel at the beginning of the expansion stroke. The air was compressed under the same conditions as the first case.

There were approximately four hundred species involved in the chemical mechanism used, therefore a decision of what species to analyze became very relevant. Based on the knowledge obtained from extensive research, eleven species were chosen. The analyzed species are the following: carbon dioxide ( $\text{CO}_2$ ), water ( $\text{H}_2\text{O}$ ), carbon monoxide ( $\text{CO}$ ), monatomic hydrogen ( $\text{H}$ ), diatomic hydrogen ( $\text{H}_2$ ), ozone ( $\text{O}_3$ ), monatomic oxygen ( $\text{O}$ ), diatomic ( $\text{O}_2$ ), hydroxyl ( $\text{OH}$ ), acetylene ( $\text{C}_2\text{H}_2$ ), and propargyl radical ( $\text{C}_3\text{H}_3$ ).

## 4.2 Results and Discussion

**Concentration trends of  $\text{H}_2\text{O}$  and  $\text{H}_2$ .**  $\text{H}_2\text{O}$  is a complete combustion product; while,  $\text{H}_2$  is an intermediate that is formed between the decomposition of the fuel and the formation of  $\text{H}_2\text{O}$ . The concentrations of  $\text{H}_2\text{O}$  and  $\text{H}_2$  peaked at the point of ignition. However after ignition, concentrations were unaffected by the change in speed and the different levels of ozone. The actual trends of these species are shown in Figure 4.1.

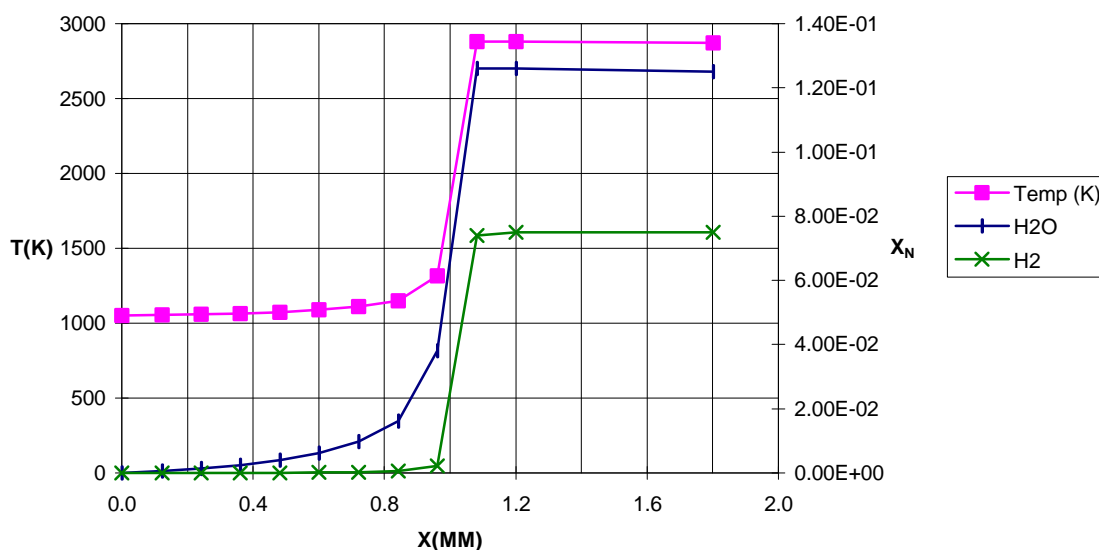
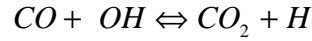


Figure 4.1: The concentration of  $\text{H}_2\text{O}$  and  $\text{H}_2$  as a function of position in the expansion stroke at any of the three speeds and eight levels of ozone. Trends shown start at top dead center and end shortly after ignition.

**Concentration of  $\text{CO}_2$  and  $\text{CO}$ .**  $\text{CO}_2$  and  $\text{CO}$  are products of any hydrocarbon oxidation. Their evolution is an immediate consequence of the attack of the soot and oxidation of intermediate products. The oxidation of  $\text{CO}$  is known as the bottleneck reaction. (See reaction below).



This reaction is the slowest reaction in the mechanism and is very important because it is the rate determining reaction.

In the Senkin simulations, the concentration of  $CO_2$  and  $CO$  exhibited different uniform trends after ignition (See Figures 4.2 and 4.3).  $CO_2$  quantities were minimally altered by the different levels of ozone. Figure 4.2 shows only a two percent decrease in the levels of carbon dioxide at the point of ignition when comparing the ozone level of 0 to 1000 PPM.

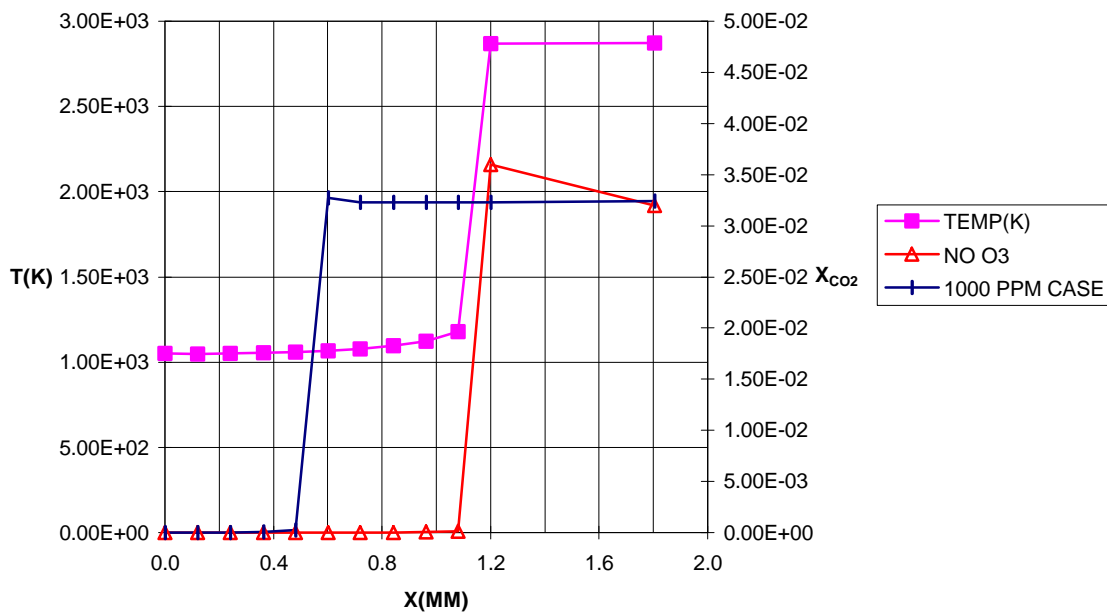


Figure 4.2: The temperature of the no ozone case and concentration of  $CO_2$  as a function of position in the expansion stroke at a speed of 1500 rpm and ozone levels of 0 PPM and 1000 PPM. Trends shown start at top dead center and end shortly after ignition.

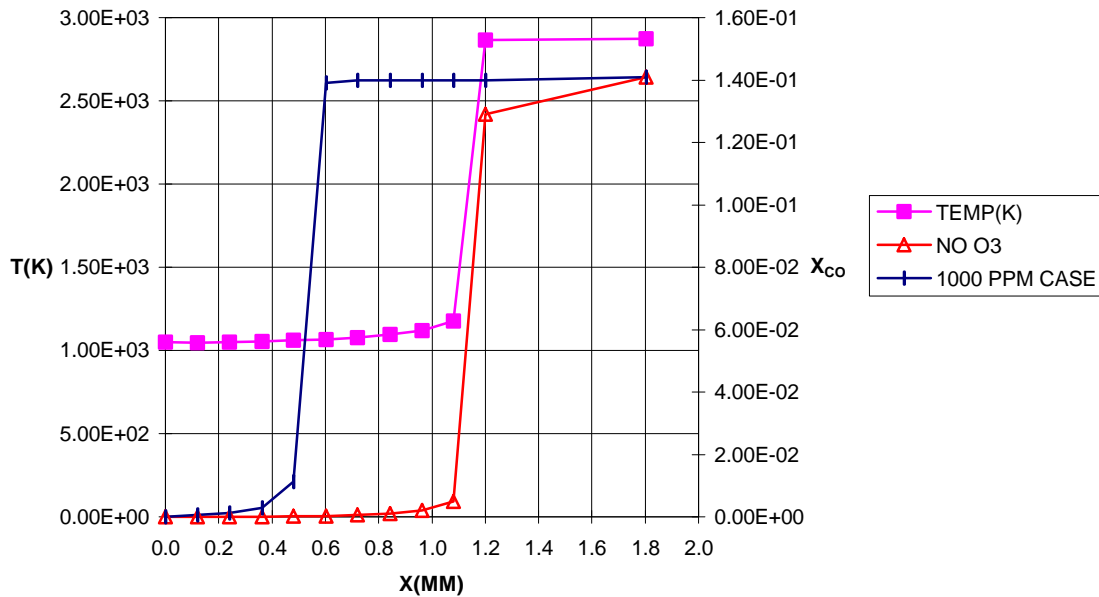


Figure 4.3: The temperature of the no ozone case and concentration of CO as a function of position in the expansion stroke at a speed of 1500 rpm and ozone levels of 0 PPM and 1000 PPM. Trends shown start at top dead center and end shortly after ignition.

The CO concentration was lower than CO<sub>2</sub> and it slightly increased at a higher level of ozone. When contrasting the two graphs, trends elucidate the formation of CO to be five times greater than CO<sub>2</sub>. This result suggest that CO is the dominant product between the two carbon species during the oxidation of hexane.

**Concentration of O<sub>3</sub>, O<sub>2</sub>, and O.** Ozone is created when an electrical discharge passes through pure oxygen gas. This charge breaks the O<sub>2</sub> bond and generates two oxygen atoms. The O atoms then bond with another O<sub>2</sub> molecule and form ozone. When ozone is decomposed, it follows a similar but reverse path.

It was observed that the amount of ozone oxidized during the expansion stroke was influenced by the injection time. When ozone was injected with the fuel (CASE B) at the beginning of the expansion stroke, it was oxidized immediately and dropped to a zero level after the first time step (See Figure 4.4).

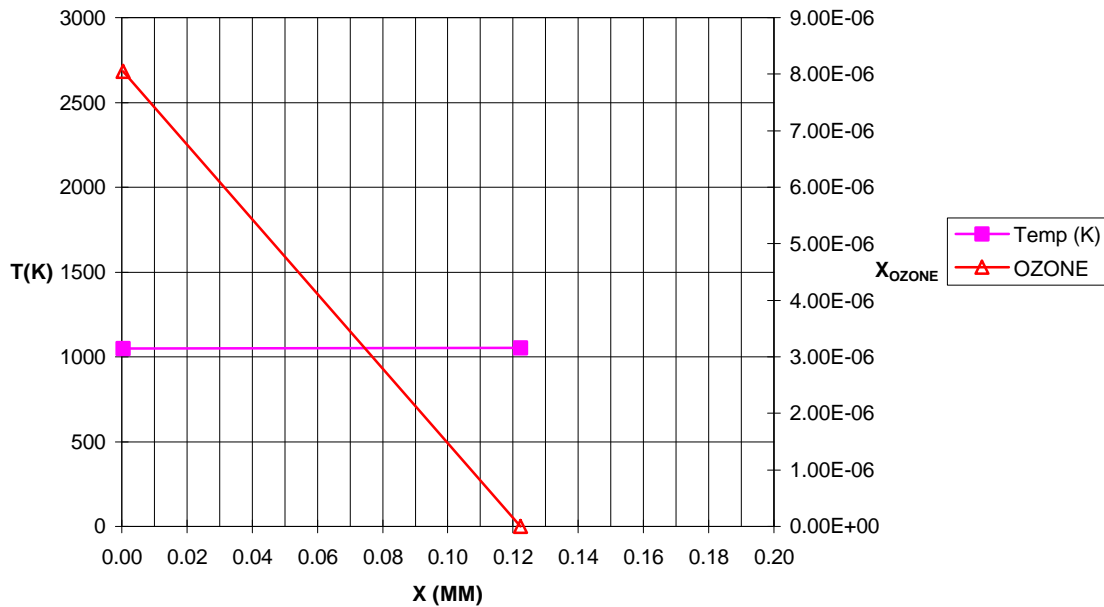


Figure 4.4: The temperature and concentration of  $O_3$  as a function of position in the expansion stroke at any of three speeds and eight ozone levels. Trends shown start at bottom dead center and end shortly after first time step.

When ozone was added with air in the beginning of the compression stroke (CASE A),  $O_3$  started to decompose at approximately 600K (See Figure 4.5). Past research suggested that the decomposition temperature of ozone is approximately 800K (Balakrishnan, 1993). At the low engine speed (1500 rpm), 66% of ozone was decomposed; while at the higher engine speed of 2500 rpm, 81% of ozone was decomposed (See Figure 4.5).

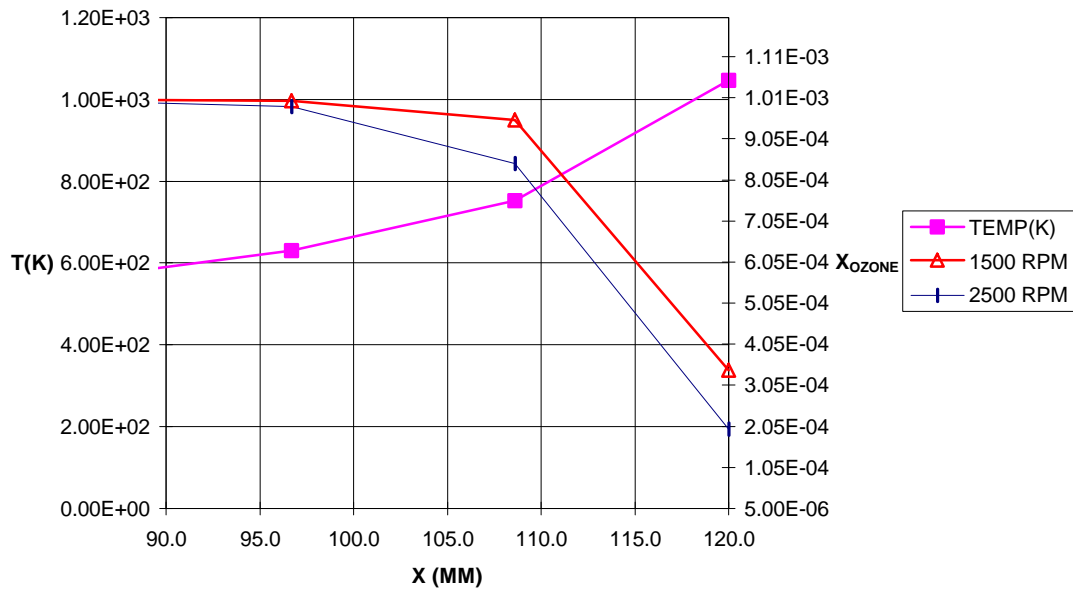


Figure 4.5: The temperature and concentration of  $O_3$  as a function of position in the compression stroke at 1500 and 2500 RPM. Ozone level is 1000 PPM. Trends shown start shortly before the decomposition of ozone and end at the top dead center.

The different percentages are a direct result of the decomposition temperature being reached faster at the higher engine speed than the lower engine speed. Therefore, the time of the decomposition of ozone depends on the speed of the engine.

Once ozone decomposes,  $O_2$  and  $O$  are formed. However, the  $O_2$  level does not change because the amount of  $O_2$  generated is very small compared to the amount that already exists in air. The concentration of  $O$  drops as quickly as it is created (See Figure 4.6 and 4.7) The trends shown are the same regardless of speed but the initial  $O$  concentration depends on the amount of ozone injected.

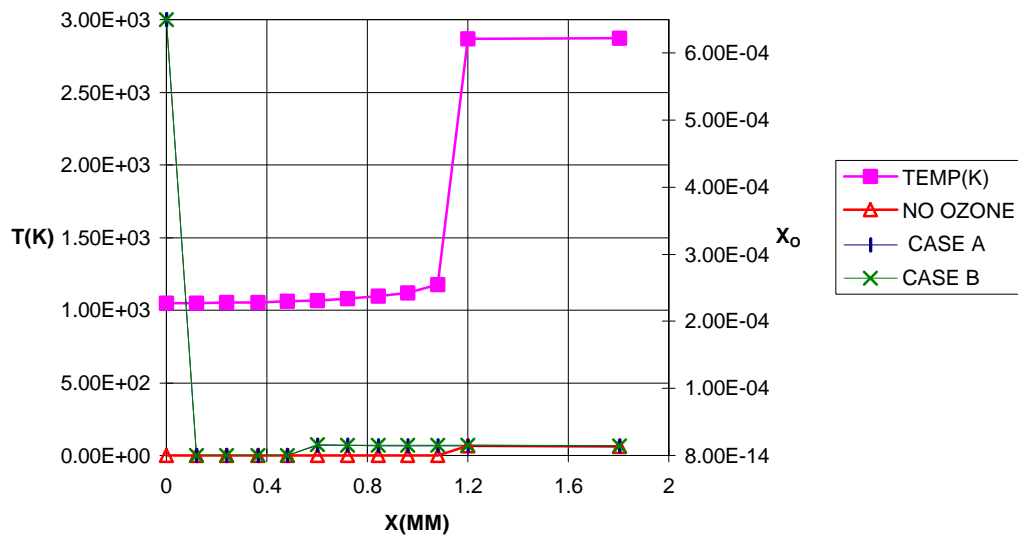


Figure 4.6: The temperature of the no ozone case and concentration of O as a function of position in the expansion stroke at an engine speed of 1500 rpm. Ozone level is 1000 PPM and all injection times are displayed. Trends shown start at top dead center and end shortly after ignition.

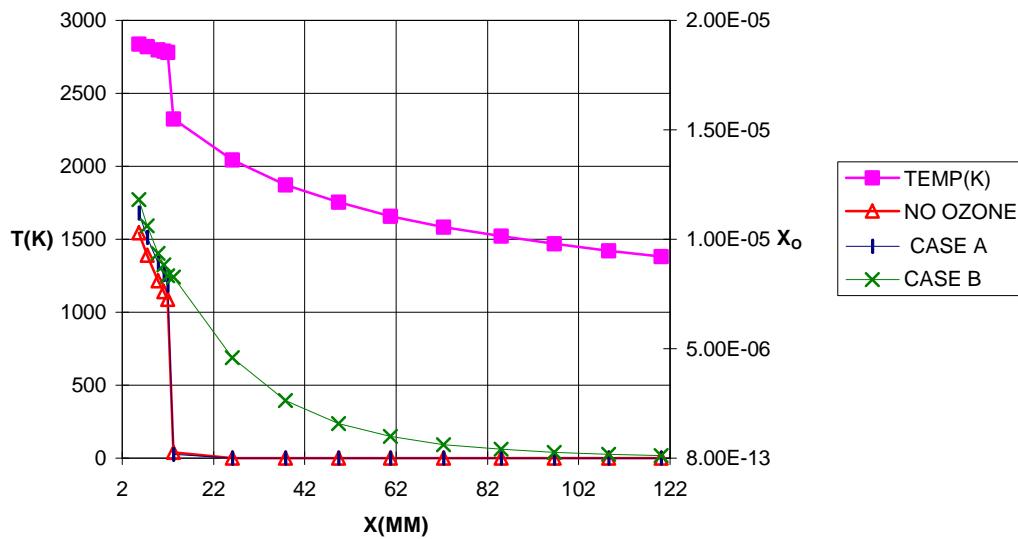


Figure 4.7: The temperature of the no ozone case and concentration of O as a function of position in the expansion stroke at an engine speed of 1500 rpm. Ozone level is 1000 PPM and all injection times are displayed. Trends shown start at shortly after ignition and end bottom dead center

**Concentration of H.** The concentration of H is a key contributor to soot formation. When the H radical is subjoined with acetylene, the outcome is the formation of vinyl acetylene. This species is one of the first species to be form and its formation leads to the generation of the first aromatic ring. When the H radical bonds with an O atom, it can also contributes to the formation of the OH radical.

The concentrations of H were fairly consistent throughout the analysis. The H concentration peaked at the time of ignition and exhibited depleting trends thereafter, regardless of the engine speed, time, and level of ozone injected (See in Figure 4.6). Although, there was a slight increase in quantities at the higher engine speed. Shortly after ignition, the H concentration decreased with respect to time during the expansion stroke.

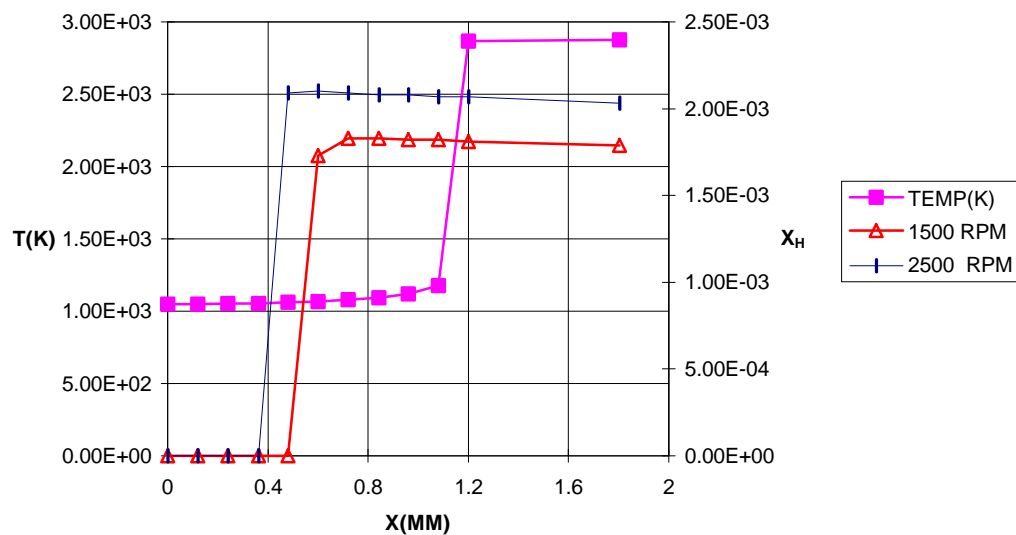


Figure 4.8: The temperature of the no ozone case and concentration of H as a function of the position of the expansion stroke at engine speeds of 1500 and 2500 rpm for any ozone level and injection time. Trends shown start at top dead center and end shortly after ignition.

**Concentration of OH.** The OH radical is a strong oxidizer that delays the formation of soot precursors. The concentration of OH depends on the temperature and oxygen concentration in the oxidizer or fuel (Aftel et al, 1988). Hence, the level of OH produced during this simulation should be greatly influenced by the level and the time of ozone injection. The OH concentration climaxed at the time of ignition and generated decreasing trends thereafter regardless of engine speed, time, and level of ozone injected (See Figure 4.9 - 4.20).

The OH concentration peaked at the time of ignition and the largest ignition concentration occurred at the no ozone case. This result was possible because the burning rate of a hydrocarbon is proportional to the fraction of oxygen available. The no ozone case had the smallest amount of oxygen therefore, the ignition time for this case was a little longer. As a result of this longer time, the initial OH concentration has more time to form during the preliminary reactions that occurs before ignition at the lower injection levels. This period before ignition is called the delay period. The OH concentration formed during this period was most likely a result of the O atoms, created from the ozone decomposition, bonding with H radicals, created from cracking reactions. During the period of premixed combustion, which begins at the point of ignition, the OH level for the no ozone case rapidly decreases. The period of premixed combustion is important because this is where fuel pyrolysis takes place and where the highest levels of OH is produce.

During the premixed combustion period, the trends of the OH concentration quickly change. There were higher levels of OH when ozone was injected with the fuel at the beginning of the expansion stroke (CASE B) than at the beginning of the compression stroke (CASE A). There was a 560% increase in OH levels at an ozone injection level of 25 PPM for CASE B compared with the no ozone case after ignition. However, a 12% reduction in the levels of OH were noticed at the same level of ozone after contrasting the no ozone case to CASE A. As the levels of ozone increased, the percentages changed slightly. For instance, at 100 PPM there was a 630% increase for CASE B and 15% reduction for CASE A; at 1000 PPM, the percentage was altered a little more. The CASE B increase was 700% while the CASE A reduction was 21%.

However, the higher engine speed results after ignition were quite different. Injection times and levels of ozone were no longer significant factors because the trends were not modified for ozone injection levels of 25 and 100 PPM. When contrasting CASE A and CASE B to the no ozone case, the percent differences were equal. Levels of 25 and 100 PPM yielded a 2% increase for the levels of OH. These same trends were exhibited at an engine speed of 2000 rpm. It can be assumed that all the OH concentration generated from the ozone injection was being used to oxidize soot precursors (See Figures 4.21 -4.44). However, the ozone injection of 1000 PPM yielded the same trends seen at 1500 rpm at the same ozone injection level (See Figure 4.18 and 4.20). In this result, it can be assumed that the higher level of ozone generated more than enough OH to reduce the formation of soot. Therefore, it can be accepted that ozone injection is more beneficial at the beginning of the expansion stroke with the fuel at the low engine speed.

Next the question of how much ozone is needed to generate a significant amount of OH will be addressed. When analyzing the percentage increase of OH at the different concentrations of ozone, it was observed that the larger amounts really did not greatly influence the OH level. Since the average ozonator available during research produces 25 PPM of ozone, its OH concentration was compared with that of 1000 PPM. ( See Figure 4.9 and Figure 4.17) It was found that 1000 PPM only yields a 10% increase in the OH level compared with 25 PPM of O<sub>3</sub>. Hence, 25 PPM would clearly be more than enough ozone to produce an effective amount of OH.

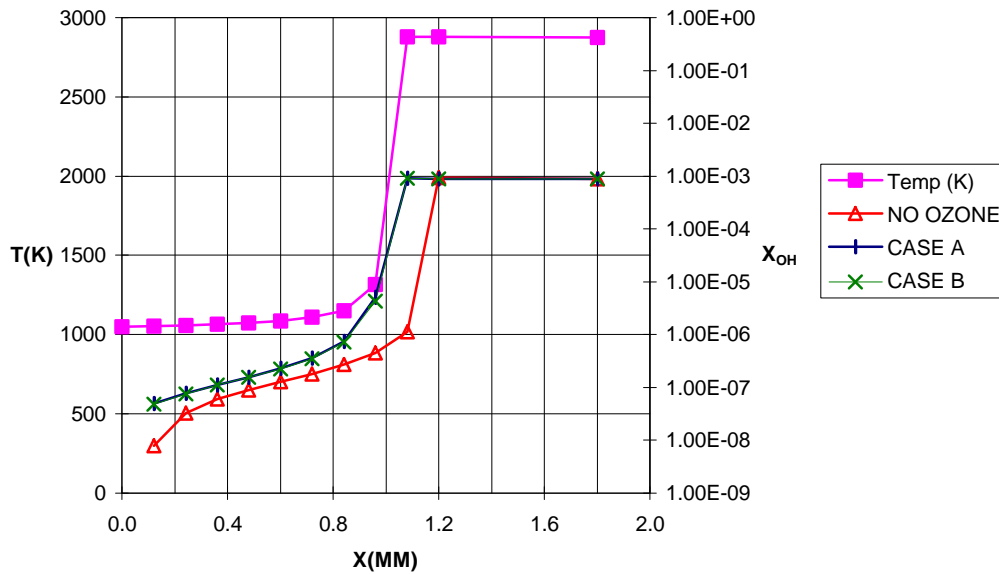


Figure 4.9: The temperature of the no ozone case and concentration of OH as a function of position in the expansion stroke at an engine speed of 1500 rpm. Ozone level is 25 PPM and all injection times are displayed. Trends shown start at top dead center and end shortly after ignition.

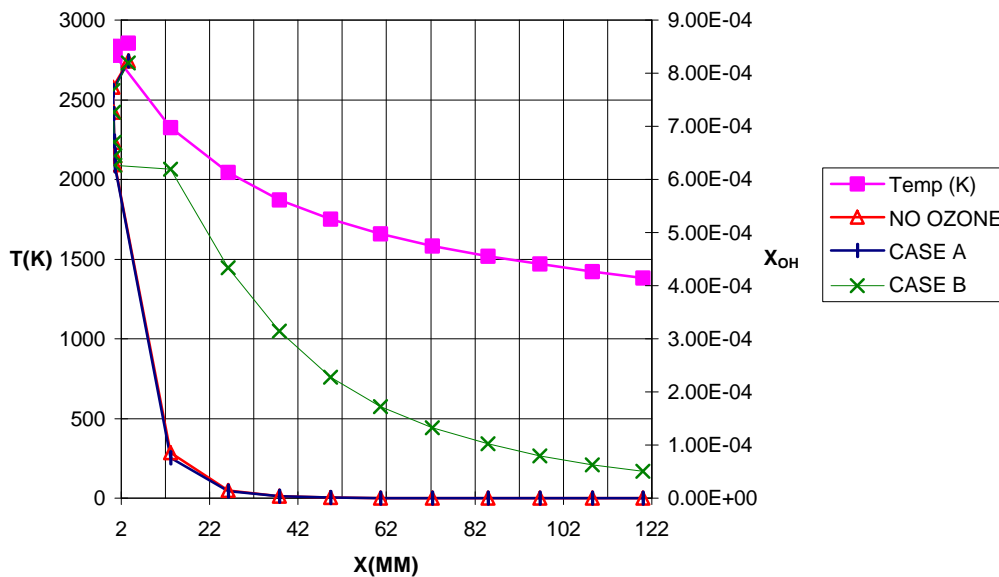


Figure 4.10 The concentration of OH as a function of position in the expansion stroke at an engine speed of 1500 rpm. Ozone level is 25 PPM and all injection times are displayed. Trends shown start shortly after ignition and end at bottom dead center.

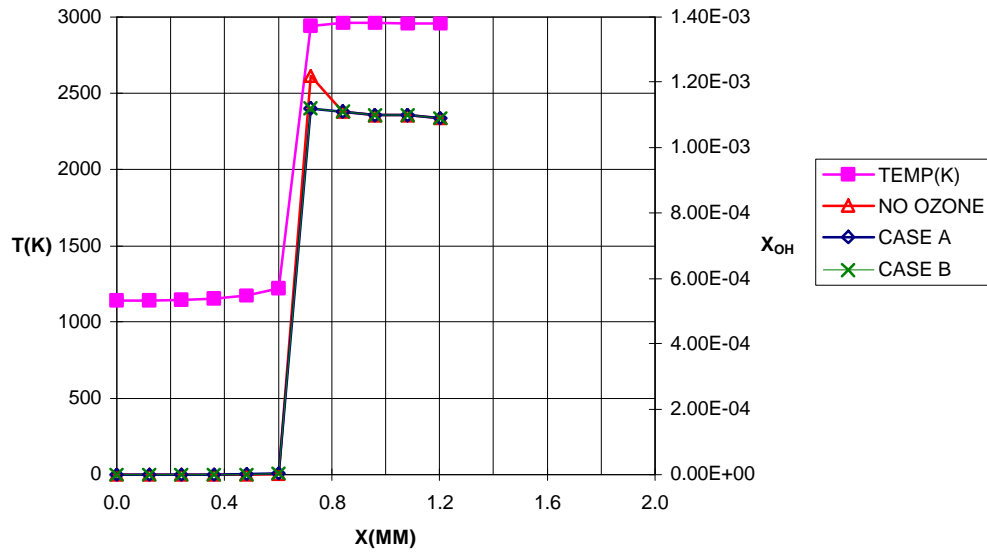


Figure 4.11: The temperature of the no ozone case and concentration of OH as a function of position in the expansion stroke at an engine speed of 2500 rpm. Ozone level is 25 PPM and all injection times are displayed. Trends shown start at top dead center and end shortly after ignition.

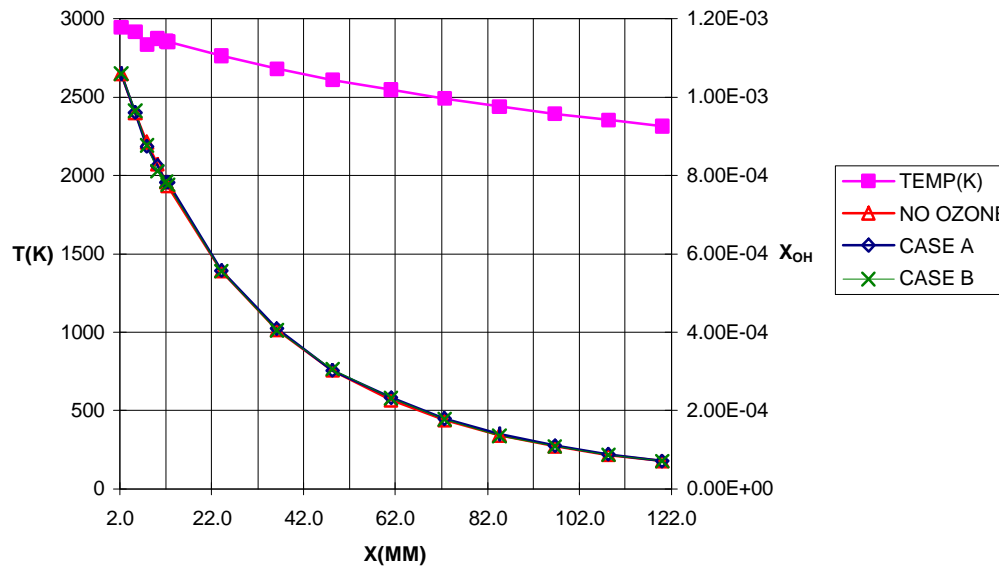


Figure 4.12: The concentration of OH as a function of position in the expansion stroke at an engine speed of 2500 rpm. Ozone level is 25 PPM and all injection times are displayed. Trends shown start shortly after ignition and end at bottom dead center.

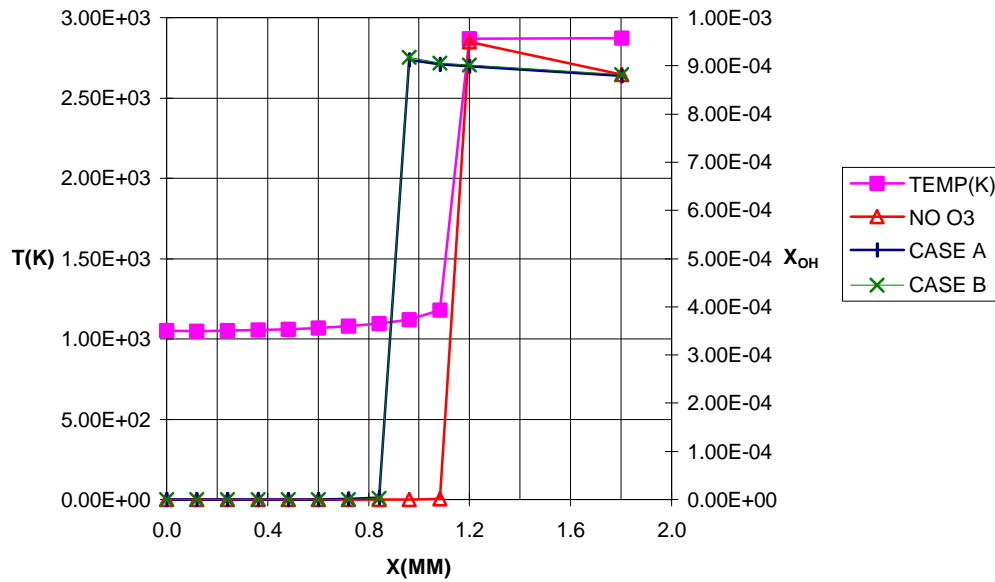


Figure 4.13: The temperature of the no ozone case and concentration of OH as a function of position in the expansion stroke at an engine speed of 1500 rpm. Ozone level is 100 PPM and all injection times are displayed. Trends shown start at top dead center and end shortly after ignition.

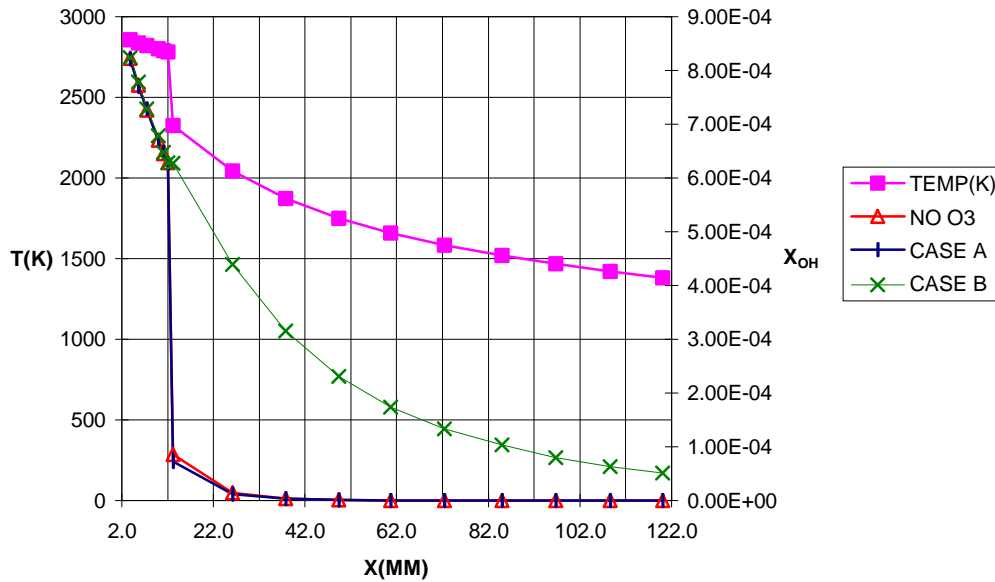


Figure 4.14: The concentration of OH as a function of position in the expansion stroke at an engine speed of 1500 rpm. Ozone level is 100 PPM and all injection times are displayed. Trends shown start at shortly after ignition and end bottom dead center

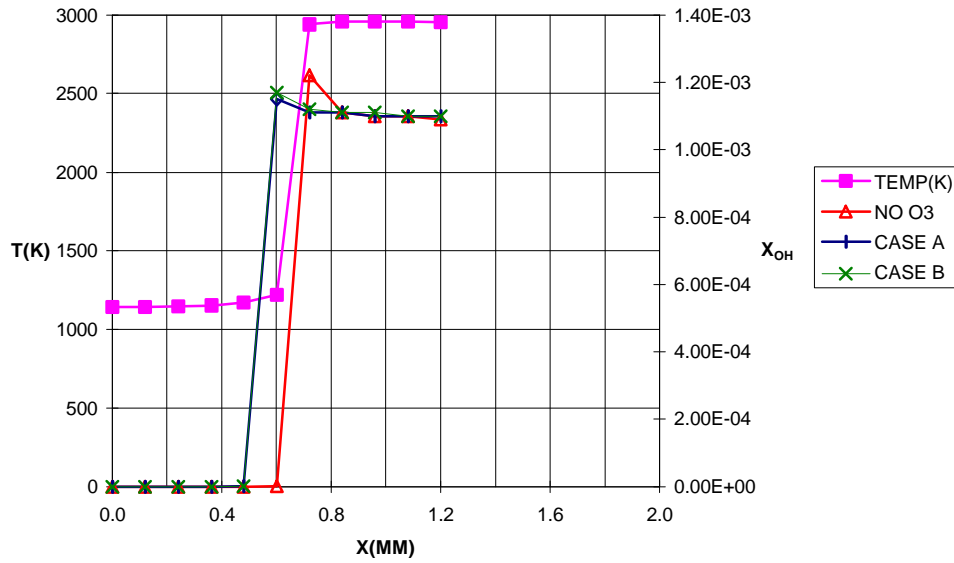


Figure 4.15: The temperature of the no ozone case and concentration of OH as a function of position in the expansion stroke at an engine speed of 2500 rpm. Ozone level is 100 PPM and all injection times are displayed. Trends shown start at top dead center and end shortly after ignition.

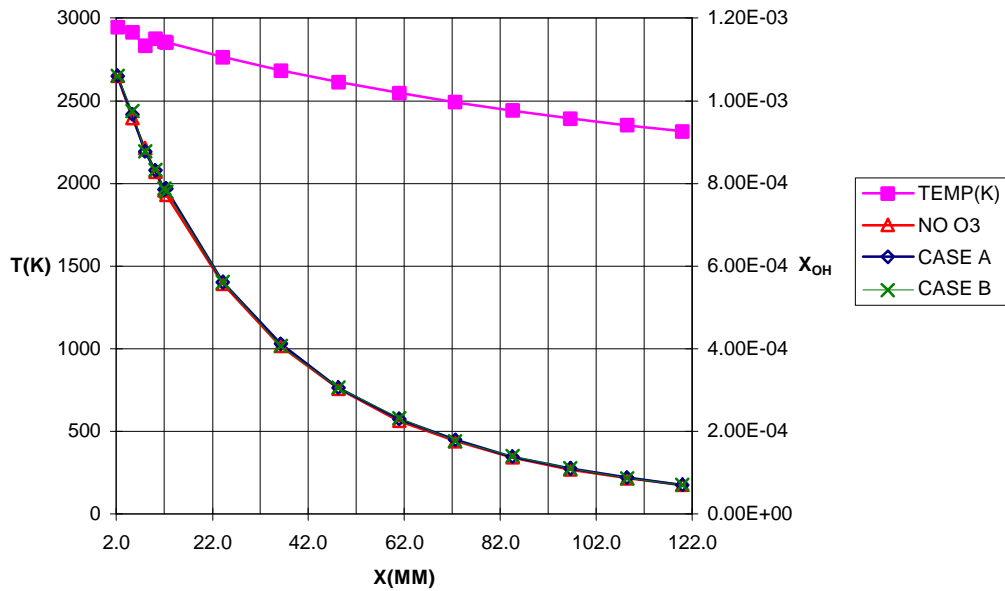


Figure 4.16 The concentration of OH as a function of position in the expansion stroke at an engine speed of 2500 rpm. Ozone level is 100 PPM and all injection times are displayed. Trends shown start at shortly after ignition and end bottom dead center

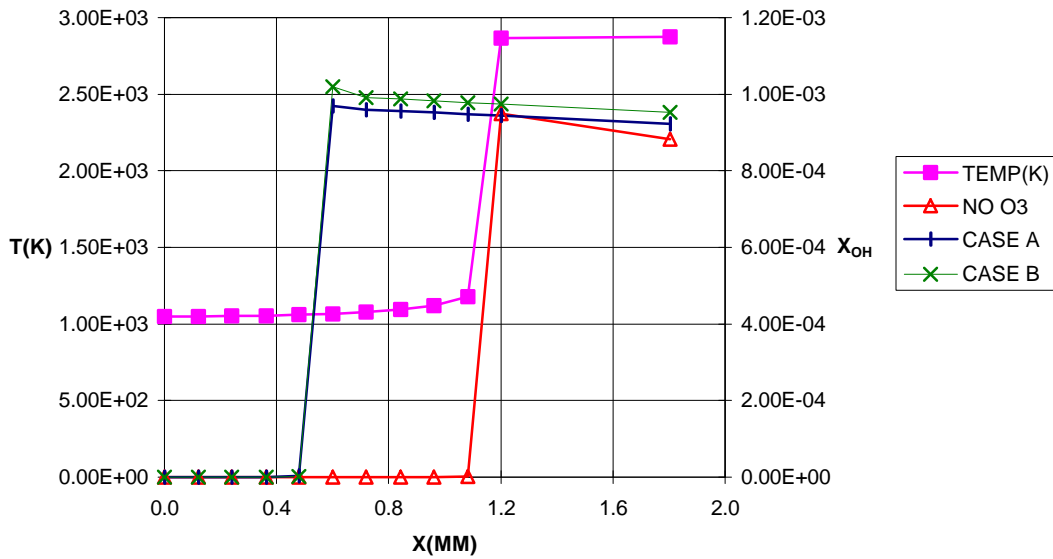


Figure 4.17: The temperature of the no ozone case and concentration of OH as a function of position in the expansion stroke at an engine speed of 1500 rpm. Ozone level is 1000 PPM and all injection time are displayed. Trends shown start at top dead center and end shortly after ignition.

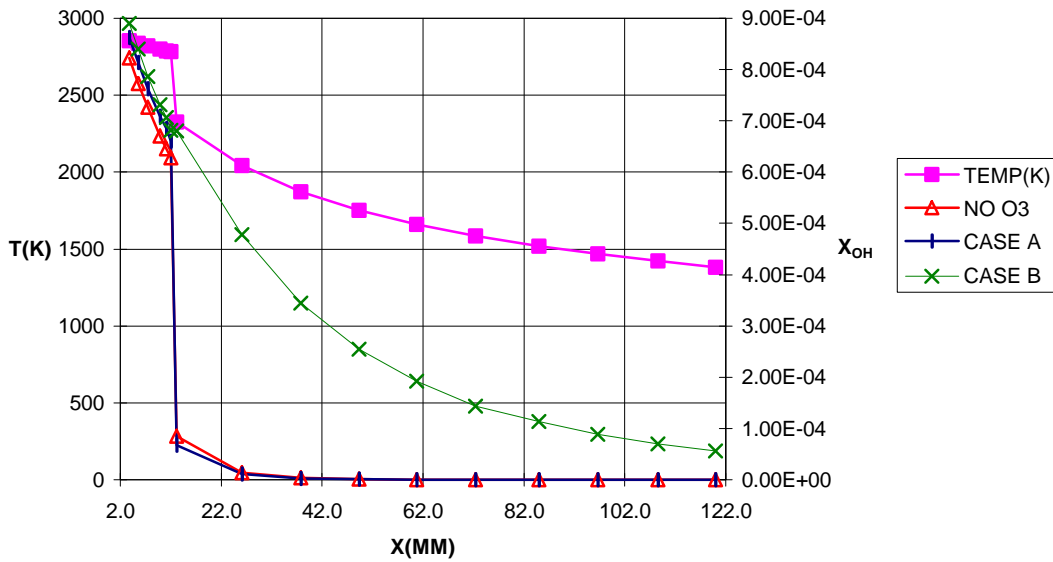


Figure 4.18: The concentration of OH as a function of position in the expansion stroke at an engine speed of 1500 rpm. Ozone level is 1000 PPM and all injection times are displayed. Trends shown start at shortly after ignition and end bottom dead center

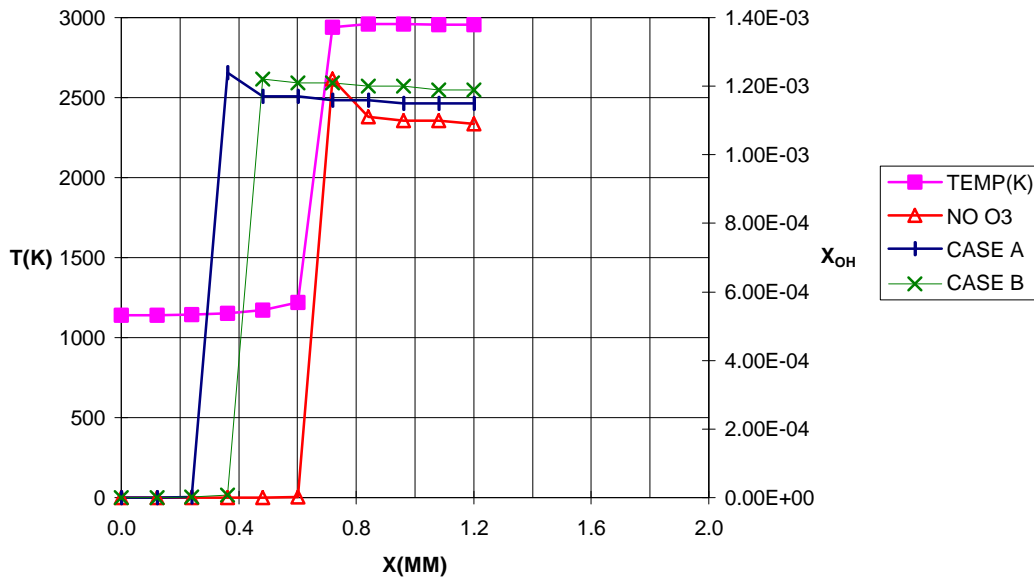


Figure 4.19: The temperature of the no ozone case and concentration of OH as a function of position in the expansion stroke at an engine speed of 2500 rpm. Ozone level is 1000 PPM and all injection times are displayed. Trends shown start at top dead center and end shortly after ignition.

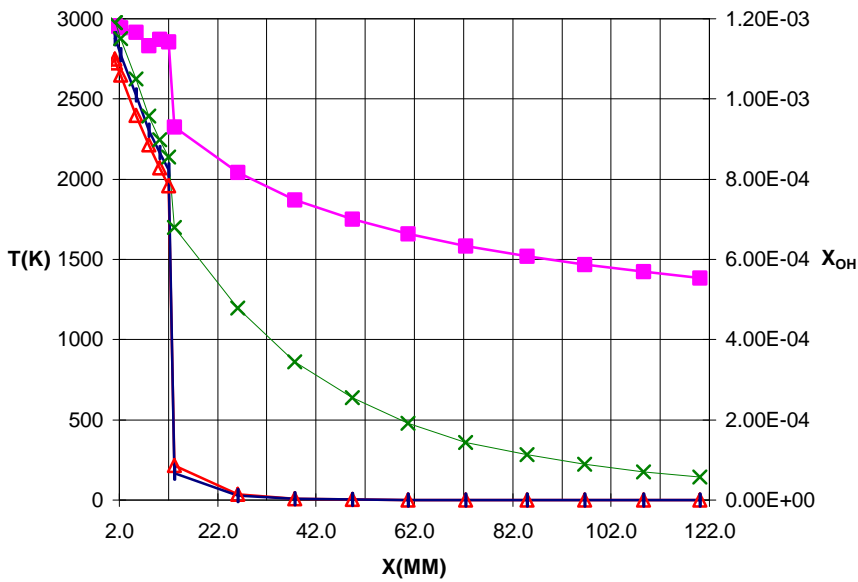


Figure 4.20: The concentration of OH as a function of position in the expansion stroke at an engine speed of 2500 rpm. Ozone level is 1000 PPM and all injection times are displayed. Trends shown start at shortly after ignition and end bottom dead center.

**Concentration of C<sub>2</sub>H<sub>2</sub>.** C<sub>2</sub>H<sub>2</sub> is a soot precursor and is the dominant growth species once soot inception has occurred due to its high concentration (Sidebotham and Glassman, 1992). C<sub>2</sub>H<sub>2</sub> is formed at 1300K and persists till 2300K (Goldberg, 1985) Similar to the previously mentioned species, the climax of the C<sub>2</sub>H<sub>2</sub> concentration occurred at the time of ignition. C<sub>2</sub>H<sub>2</sub> is an intermediate formed as a result of the pyrolysis of hexane. During the premixed combustion period, which starts with ignition, its concentration drops immediately.

The trends for the C<sub>2</sub>H<sub>2</sub> concentration shortly after ignition were small compared to the maximum concentration at ignition. In CASE B at a engine speed of 1500 rpm, C<sub>2</sub>H<sub>2</sub> levels decrease again by 30% immediately after ignition (See Figure 4.21 - 4.32). This outcome was uniform despite the different levels of ozone. When CASE B was contrasted to the no ozone case, the C<sub>2</sub>H<sub>2</sub> level decreased by two orders of magnitude; the actual reduction of C<sub>2</sub>H<sub>2</sub> was 94%. The temperature and concentration of C<sub>2</sub>H<sub>2</sub> generated decreasing trends. CASE A and the no ozone case exhibited similar trends, but the no ozone case generated slightly higher values of C<sub>2</sub>H<sub>2</sub>. (See Figure 4.21- 4.32). The C<sub>2</sub>H<sub>2</sub> concentration reached a maximum at approximately 1700K which occurs at the middle of the expansion stroke in the no ozone case and CASE A (See Figure 4.21 - 4.32). This temperature is quite significant since soot starts to form at approximately 1600K. The increasing trends must stem from error in the simulation because the formation of C<sub>2</sub>H<sub>2</sub> was generated from fuel pyrolysis; at this point, all the combusting fuel is gone. This increase in the C<sub>2</sub>H<sub>2</sub> concentration is not as big as the climax concentration at ignition therefore, these trends were not influential.

Once again, there were different observations for the engine speed of 2500 rpm after ignition. After ignition, the C<sub>2</sub>H<sub>2</sub> concentration decreases and is at its minimum at 2545 K which correspond to the middle of stroke for all levels of ozone. As the temperature continued to decreased, the level of C<sub>2</sub>H<sub>2</sub> began to increased. By the end of stroke, C<sub>2</sub>H<sub>2</sub> levels were back to 95% of its initial amount after ignition. Hexane has already pyrolyzed so the C<sub>2</sub>H<sub>2</sub> generated after ignition must come from an error in the simulation because there is no way it could possibly be formed. These trends are not significant because the minute amount of C<sub>2</sub>H<sub>2</sub> generated after ignition compared to the amount generated at ignition is negligible. The C<sub>2</sub>H<sub>2</sub> levels were unaffected by injection time.

Next the question of how much ozone is needed to significantly reduce the C<sub>2</sub>H<sub>2</sub> concentration will be addressed. When analyzing the percentage reduction of the C<sub>2</sub>H<sub>2</sub> levels at the different concentrations of ozone, it was observed that the larger amounts really did not greatly reduce the C<sub>2</sub>H<sub>2</sub> levels. It was found that the ozone injection level of 1000 PPM only yields a 20% higher reduction of the C<sub>2</sub>H<sub>2</sub> concentration when contrasted with 25 PPM ozone injection level. The ozone injection level of 25 PPM is recognized to be an effective amount of ozone to reduce a significant amount of the C<sub>2</sub>H<sub>2</sub> concentration.

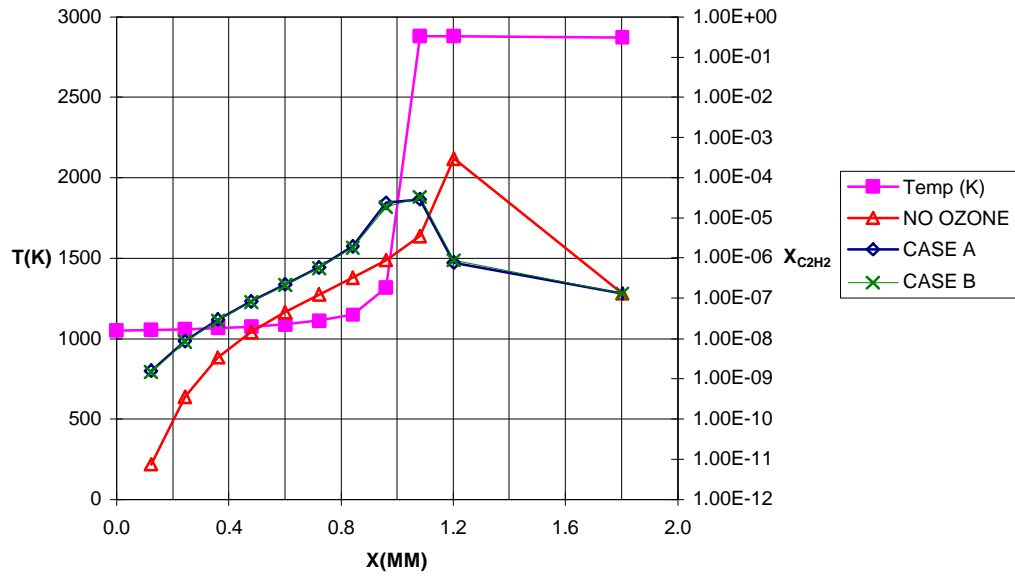


Figure 4.21: The temperature of the no ozone case and concentration of  $C_2H_2$  as a function of position in the expansion stroke at an engine speed of 1500 rpm. Ozone level is 25 PPM and all injection times are displayed. Trends shown start at top dead center and end shortly after ignition.

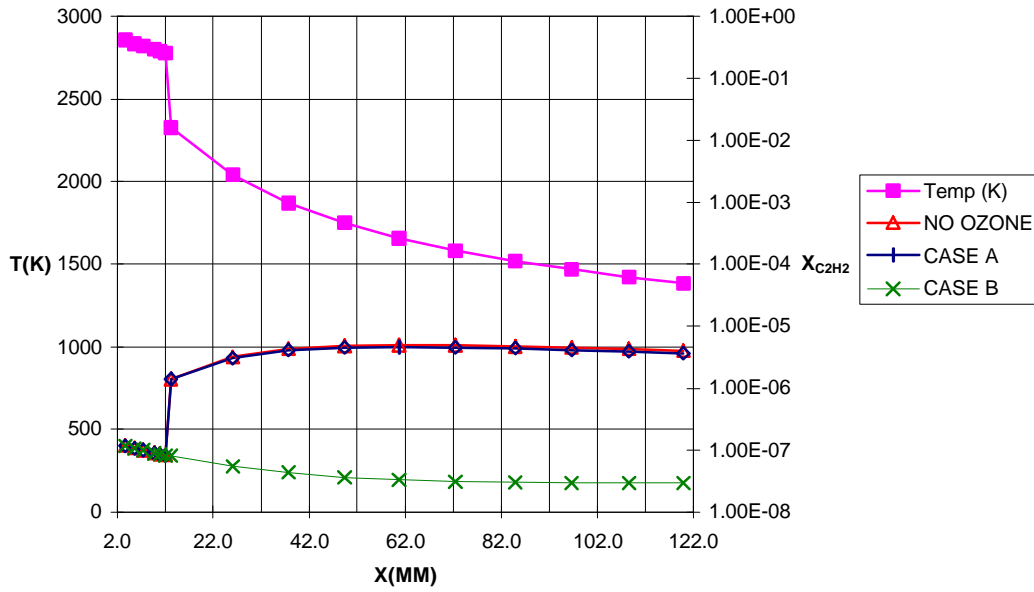


Figure 4.22: The concentration of  $C_2H_2$  as a function of position in the expansion stroke at an engine speed of 1500 rpm. Ozone level is 25 PPM and all injection times are displayed. Trends shown start shortly after ignition and end at bottom dead center.

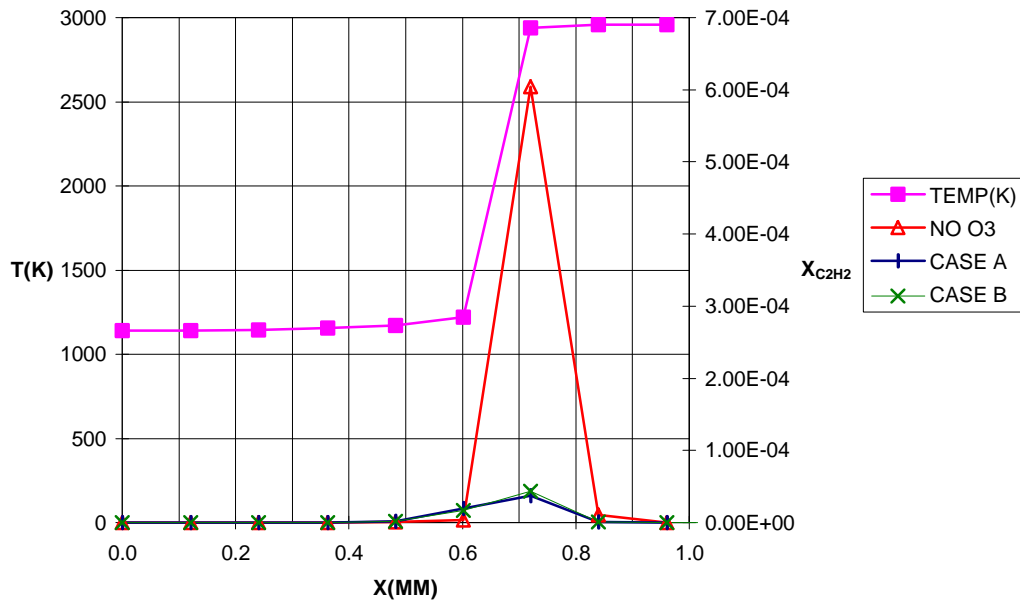


Figure 4.23: The temperature of the no ozone case and concentration of  $C_2H_2$  as a function of position in the expansion stroke at an engine speed of 2500 rpm. Ozone level is 25 PPM and all injection times are displayed. Trends shown start at top dead center and end shortly after ignition.

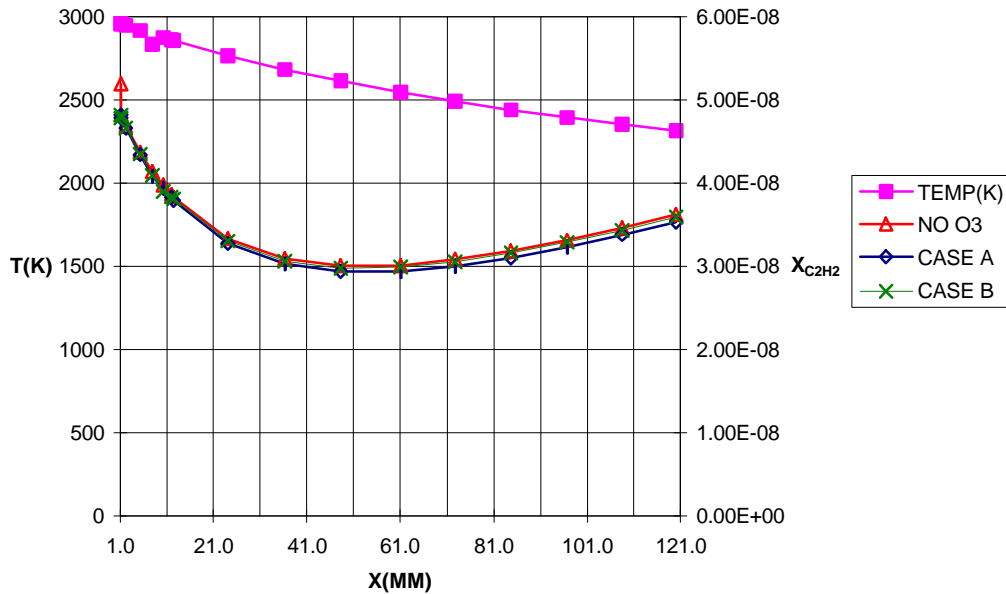


Figure 4.24: The concentration of  $C_2H_2$  as a function of position in the expansion stroke at an engine speed of 2500 rpm. Ozone level is 25 PPM and all injection times are displayed. Trends shown start shortly after ignition and end at bottom dead center.

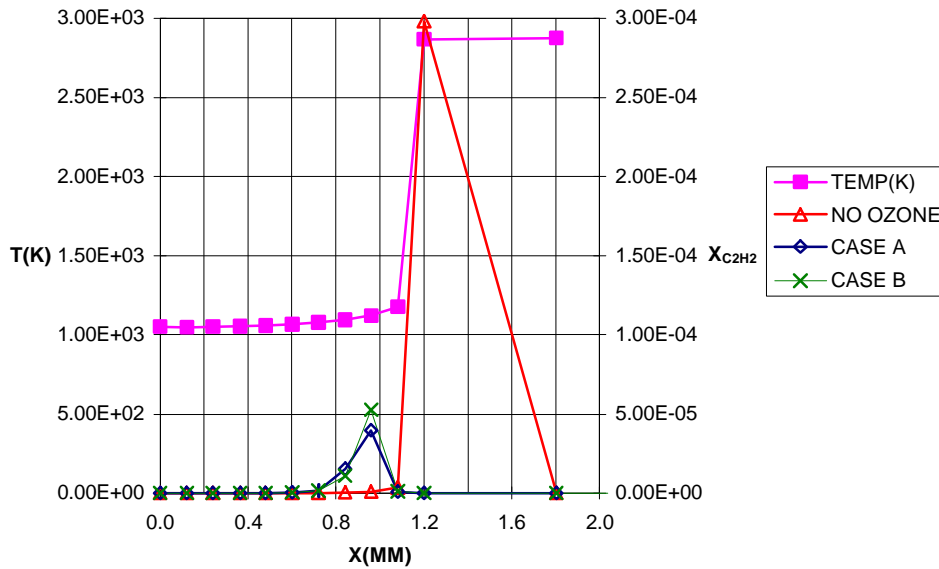


Figure 4.25: The temperature of the no ozone case and concentration of  $C_2H_2$  as a function of position in the expansion stroke at an engine speed of 1500 rpm. Ozone level is 100 PPM and all injection times are displayed. Trends shown start at top dead center and end shortly after ignition.

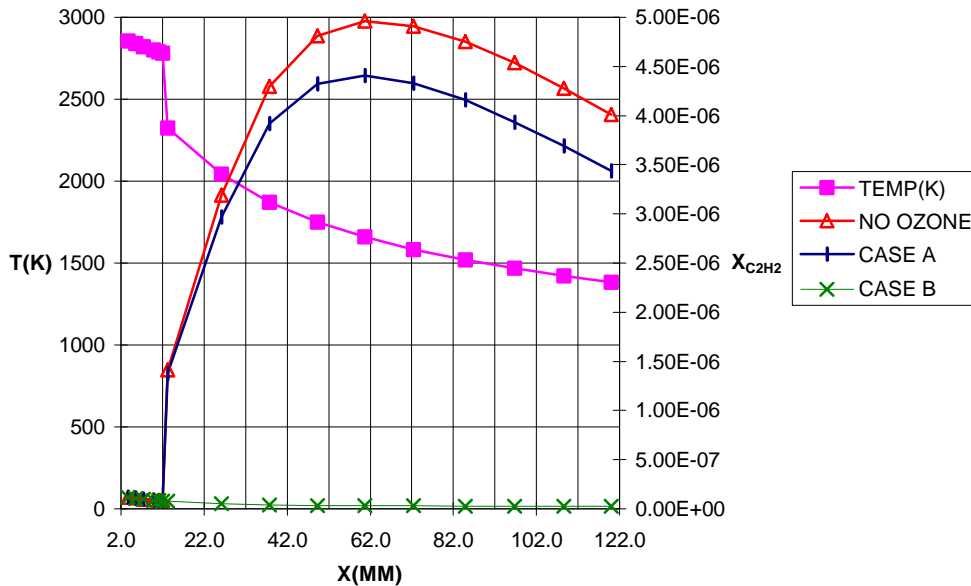


Figure 4.26: The concentration of  $C_2H_2$  as a function of position in the expansion stroke at an engine speed of 1500 rpm. Ozone level is 100 PPM and all injection times are displayed. Trends shown start shortly after ignition and end at bottom dead center.

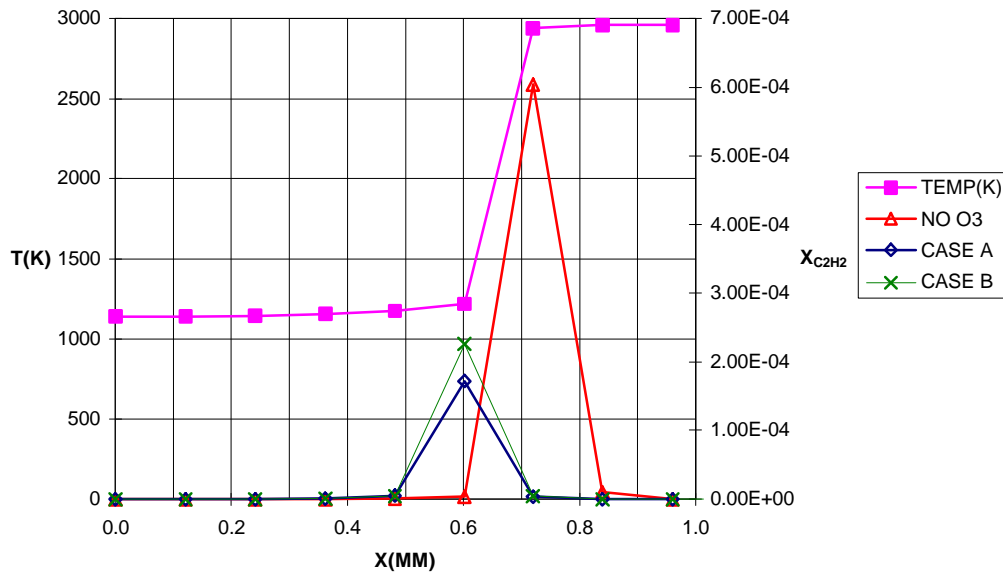


Figure 4.27: The temperature of the no ozone case and concentration of  $C_2H_2$  as a function of position in the expansion stroke at an engine speed of 2500 rpm. Ozone level is 100 PPM and all injection times are displayed. Trends shown start at top dead center and end shortly after ignition.

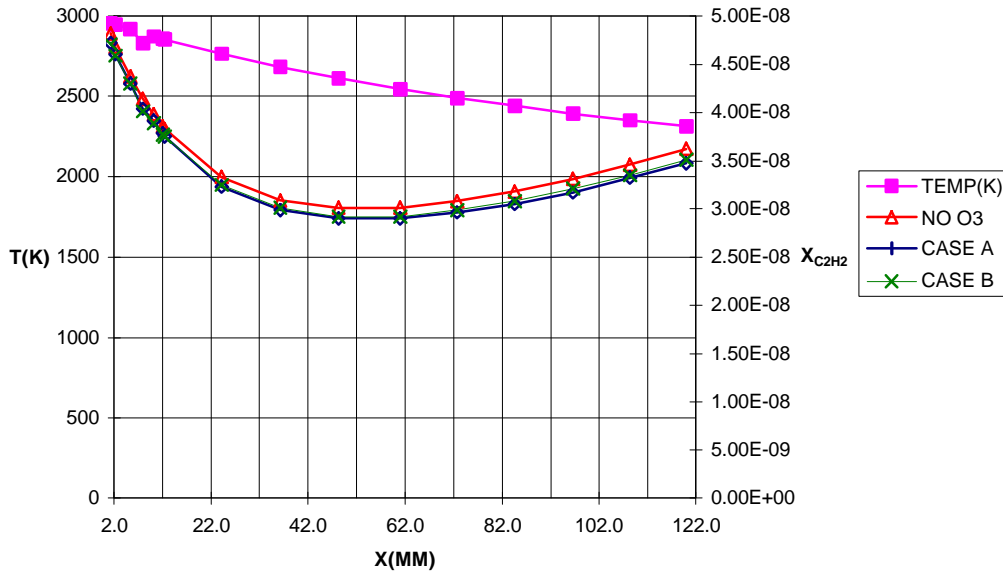


Figure 4.28: The concentration of  $C_2H_2$  as a function of position in the expansion stroke at an engine speed of 2500 rpm. Ozone level is 100 PPM and all injection times are displayed. Trends shown start shortly after ignition and end at bottom dead center.

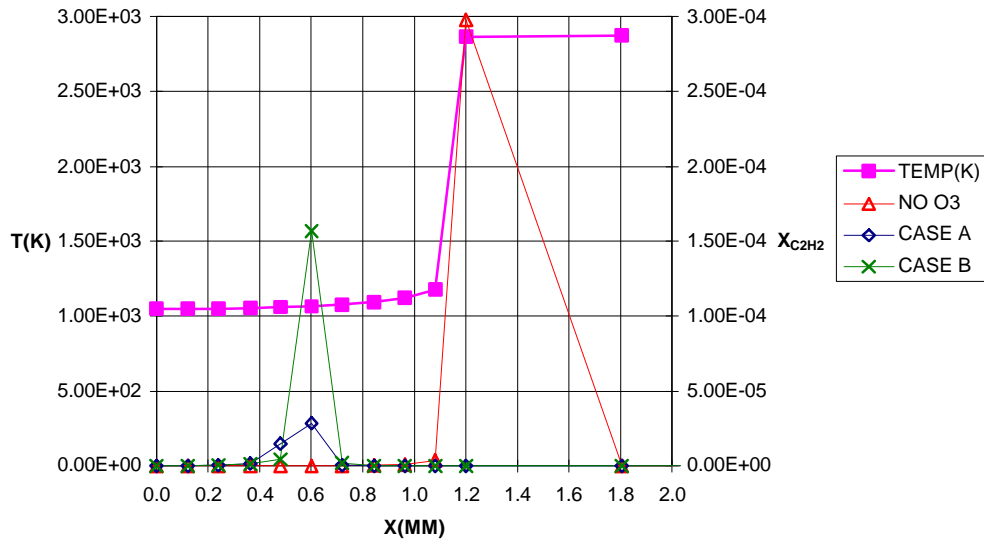


Figure 4.29: The temperature of the no ozone case and concentration of  $C_2H_2$  as a function of position in the expansion stroke at an engine speed of 1500 rpm. Ozone level is 1000 PPM and all injection times are displayed. Trends shown start at top dead center and end shortly after ignition.

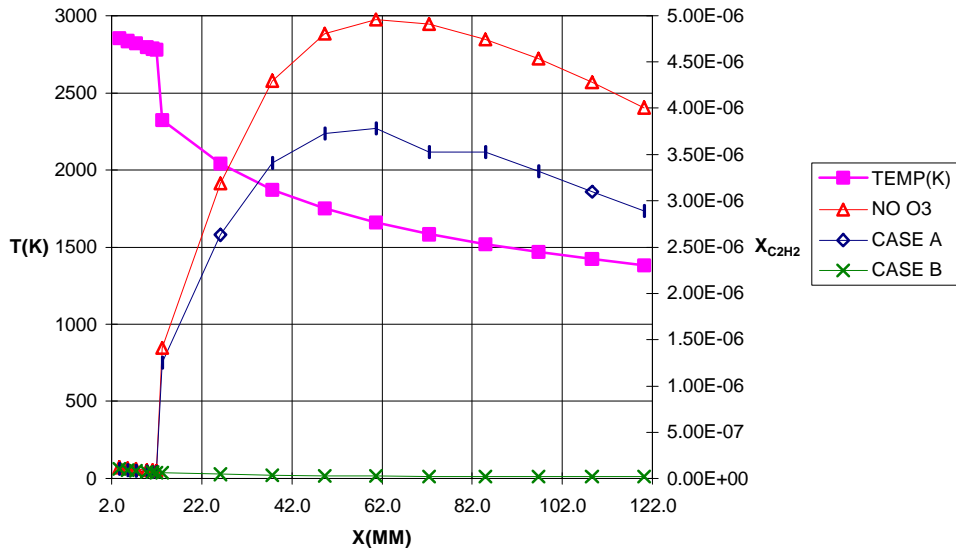


Figure 4.30: The concentration of  $C_2H_2$  as a function of position in the expansion stroke at an engine speed of 1500 rpm. Ozone level is 1000 PPM and all injection times are displayed. Trends shown start shortly after ignition and end at bottom dead center.

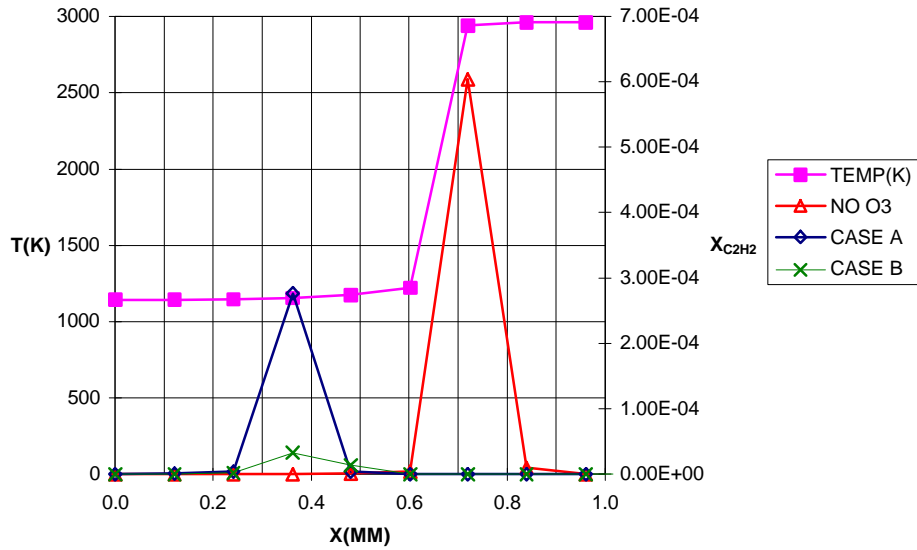


Figure 4.31: The temperature of the no ozone case and concentration of  $C_2H_2$  as a function of position in the expansion stroke at an engine speed of 2500 rpm. Ozone level is 1000 PPM and all injection times are displayed. Trends shown start at top dead center and end shortly after ignition.

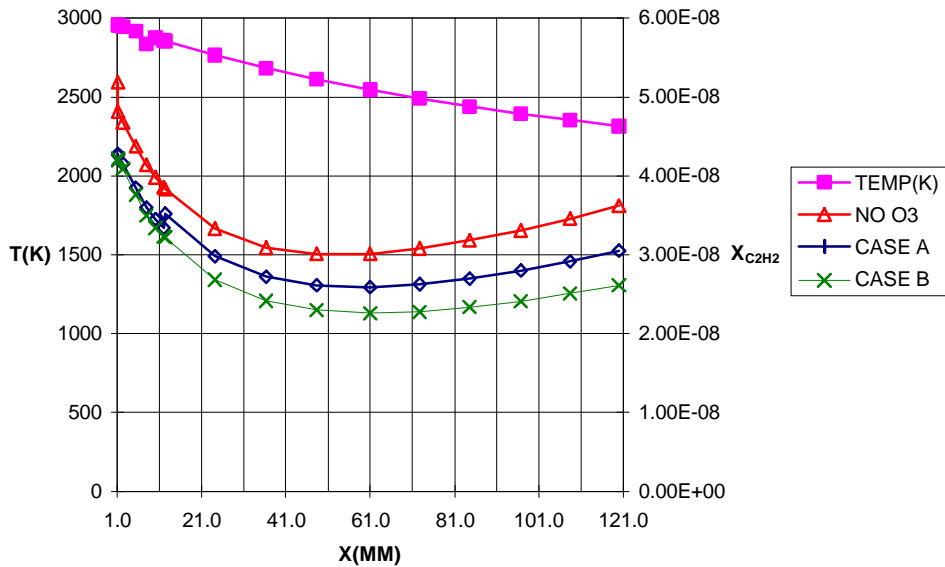


Figure 4.32: The concentration of  $C_2H_2$  as a function of position in the expansion stroke at an engine speed of 2500 rpm. Ozone level is 1000 PPM and all injection times are displayed. Trends shown start shortly after ignition and end at bottom dead center.

**Concentration of  $C_3H_3$ .**  $C_3H_3$  is an intermediate known to generate more soot because it is highly reactive.  $C_3H_3$  is a dominant soot contributor due to the fact it has no weak bonds and the recombination reactions are reversible. Past research had also found that if the decomposition of fuel is affected by the presence of the OH radical, soot is being formed from  $C_3H_3$  species (Sidebotham and Glassman, 1992). The maximum  $C_3H_3$  level occurred at ignition.  $C_3H_3$  is an intermediate formed from the pyrolysis of combusting fuel. After the premixed combustion period, its concentration drops immediately.

The lower engine speed after ignition exhibited results similar to  $C_2H_2$  previously discussed. In CASE B,  $C_3H_3$  levels decrease immediately between the first and second position after ignition by 37%. The reduction continued throughout the expansion stroke with a 99% reduction. The temperature and concentration of  $C_3H_3$  displayed decreasing trends. Once again, CASE A and no ozone case trends resemble each other. The  $C_3H_3$  levels of CASE A and the no ozone case increased immediately, yielding a 300% increase between the first and second position after ignition. This growth proceeded until the end of the expansion stroke for all levels of ozone.

The higher engine speed of 2500 rpm had uniform patterns at all levels and injection times of ozone. The  $C_3H_3$  minimum concentration occurred in the middle of stroke at approximately 2500K. By the end of stroke,  $C_3H_3$  level was back to 87% of its initial amount. The increase in the  $C_3H_3$  concentration seen at both engine speeds is negligible because the amounts generated are very small compared to the amounts formed at ignition. When comparing the concentration of  $C_3H_3$  at 25 and 1000 PPM, a reduction of 30% was observed ( See Figure 4.33 and Figure 4.41).

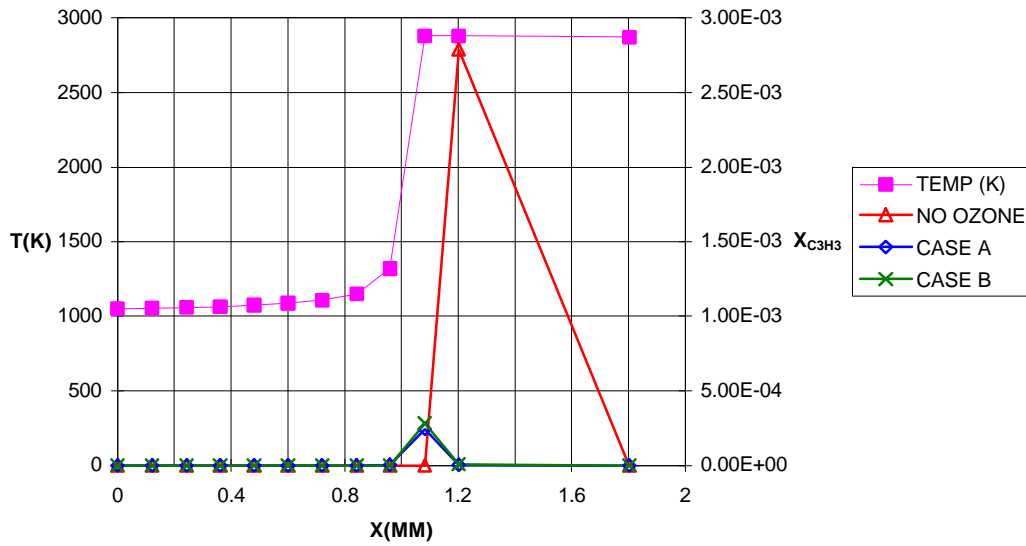


Figure 4.33: The temperature of the no ozone case and concentration of  $C_3H_3$  as a function of position in the expansion stroke at an engine speed of 1500 rpm. Ozone level injected 25 PPM and all injection times are displayed. Trends shown start at top dead center and end shortly after ignition.

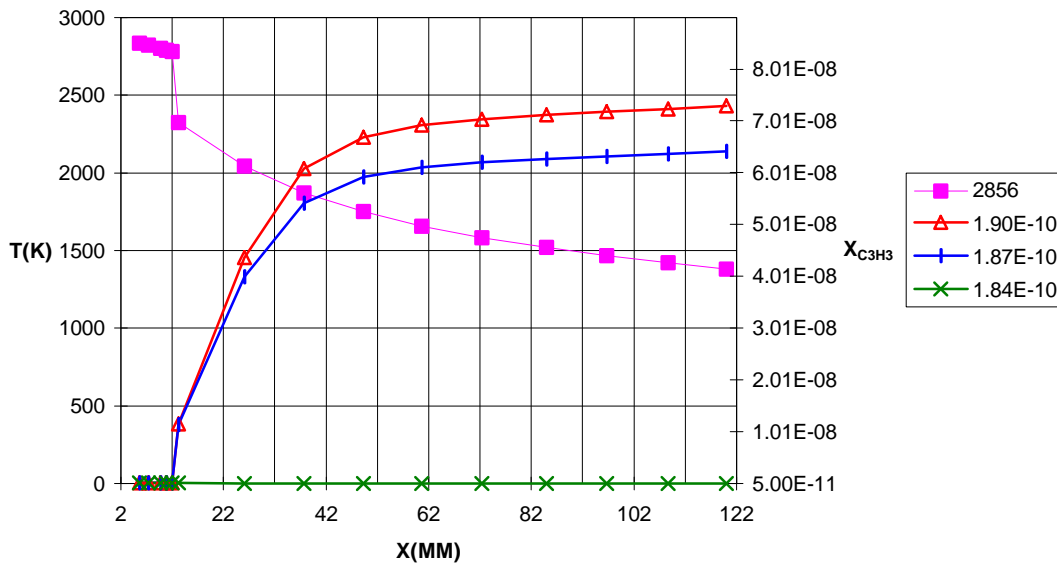


Figure 4.34: The concentration of  $C_3H_3$  as a function of position in the expansion stroke at an engine speed of 2500 rpm. Ozone level injected 25 PPM and all injection times are displayed. Trends shown start at top dead center and end shortly after ignition

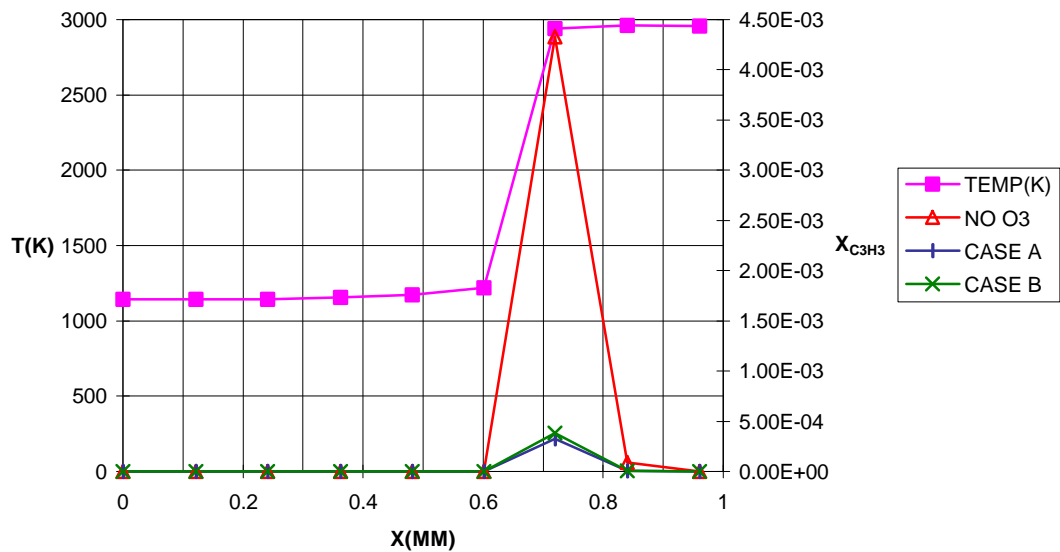


Figure 4.35: The temperature of the no ozone case and concentration of  $C_3H_3$  as a function of position in the expansion stroke at an engine speed of 2500 rpm. Ozone level injected 25 PPM and all injection times are displayed. Trends shown start at top dead center and end shortly after ignition.

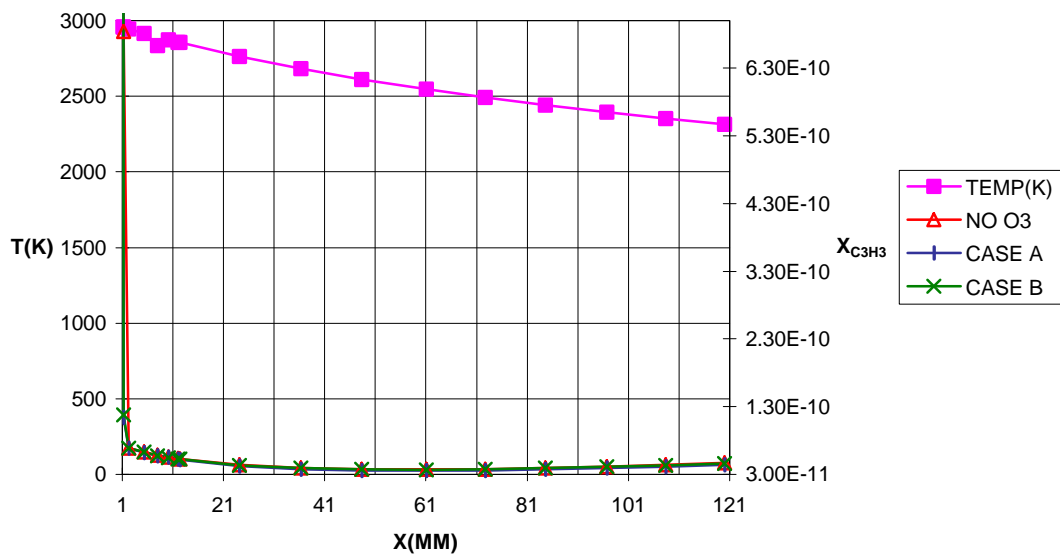


Figure 4.36: The concentration of  $C_3H_3$  as a function of position in the expansion stroke at an engine speed of 2500 rpm. Ozone level injected 25 PPM and all injection times are displayed. Trends shown start shortly after ignition and end at bottom dead center.

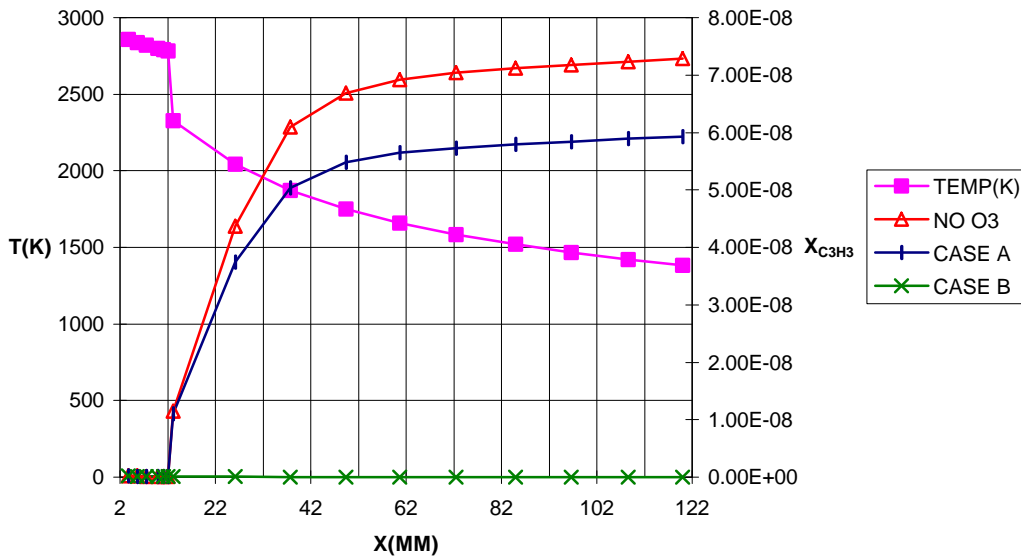


Figure 4.37: The temperature of the no ozone case and concentration of  $C_3H_3$  as a function of position in the expansion stroke at an engine speed of 1500 rpm. Ozone level injected 100 PPM and all injection times are displayed. Trends shown start at top dead center and end shortly after ignition.

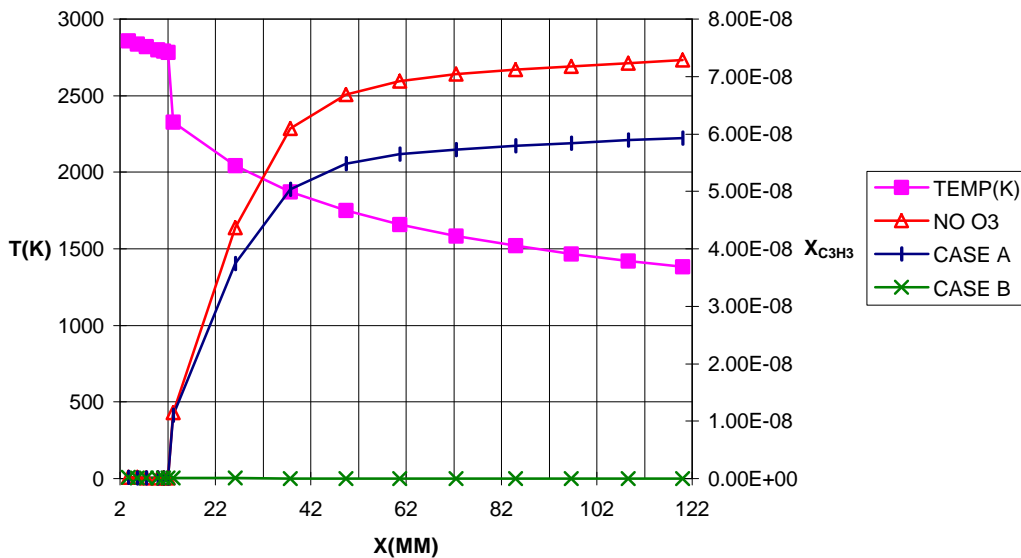


Figure 4.38: The concentration of  $C_3H_3$  as a function of position in the expansion stroke at an engine speed of 1500 rpm. Ozone level injected 100 PPM and all injection times are displayed. Trends shown start shortly after ignition and end at bottom dead center.

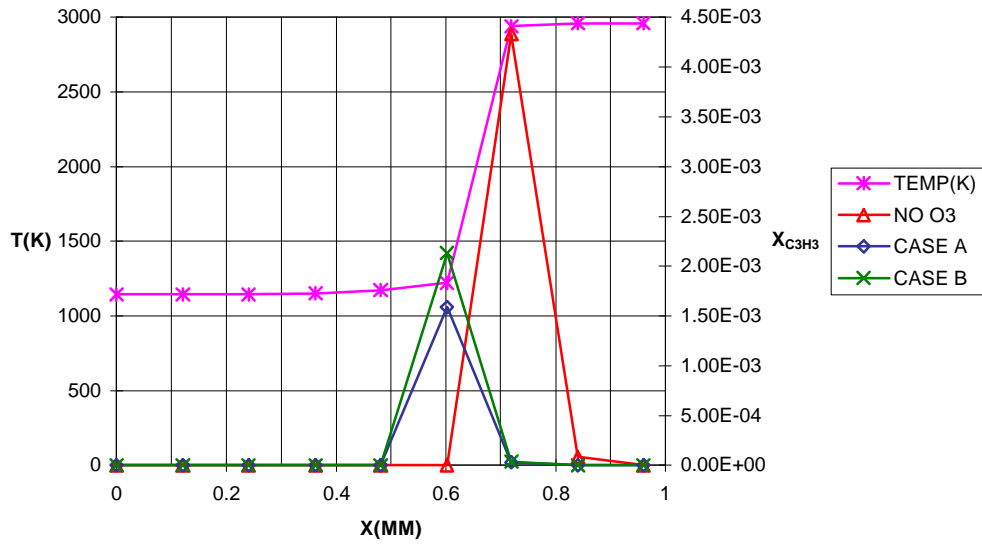


Figure 4.39: The temperature of the no ozone case and concentration of  $C_3H_3$  as a function of position in the expansion stroke at an engine speed of 2500 rpm. Ozone level injected 100 PPM and all injection times are displayed. Trends shown start at top dead center and end shortly after ignition.

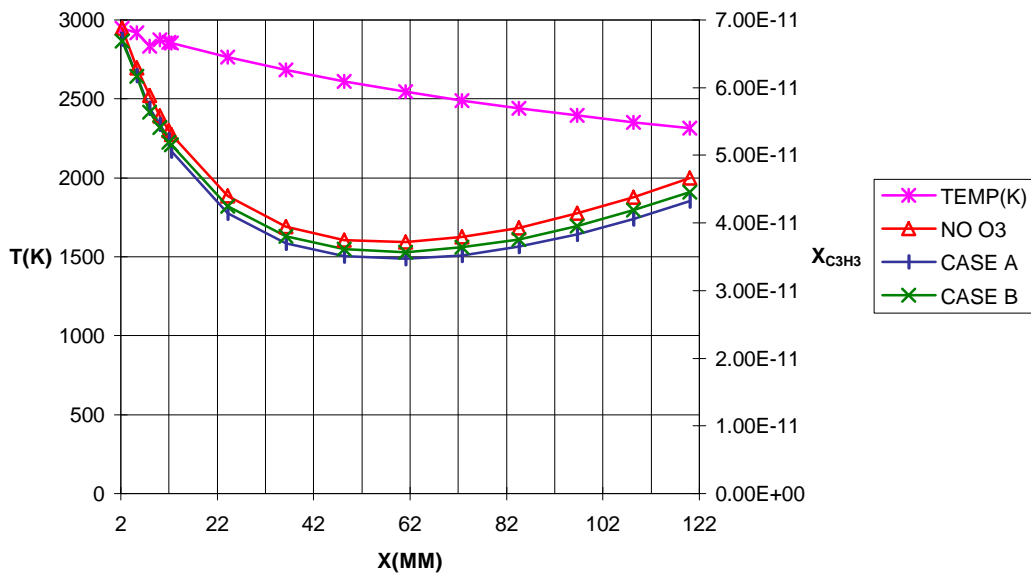


Figure 4.40: The concentration of  $C_3H_3$  as a function of position in the expansion stroke at an engine speed of 2500 rpm. Ozone level injected 100 PPM and all injection times are displayed. Trends shown start shortly after ignition and end at bottom dead center.

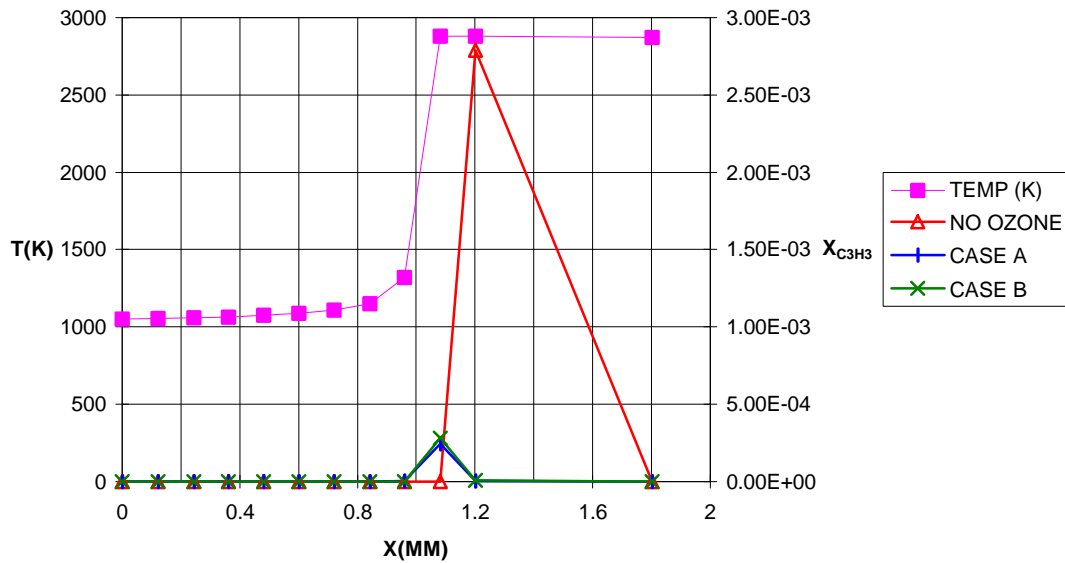


Figure 4.41: The temperature of the no ozone case and concentration of  $C_3H_3$  as a function of position in the expansion stroke at an engine speed of 1500 rpm. Ozone level injected 1000 PPM and all injection times are displayed. Trends shown start at top dead center and end shortly after ignition.

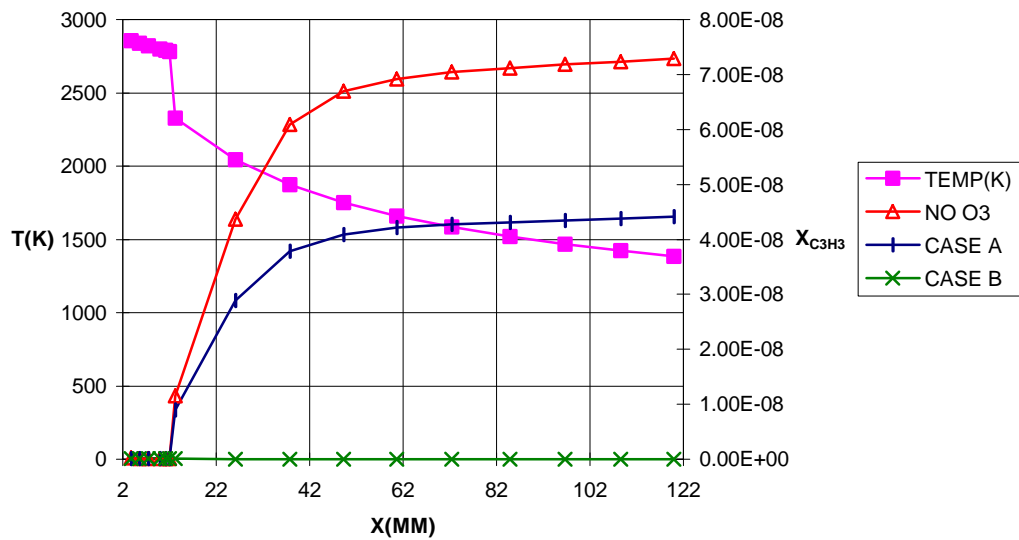


Figure 4.42: The concentration of  $C_3H_3$  as a function of position in the expansion stroke at an engine speed of 1500 rpm. Ozone level injected 1000 PPM and all injection times are displayed. Trends shown start shortly after ignition and end at bottom dead center.

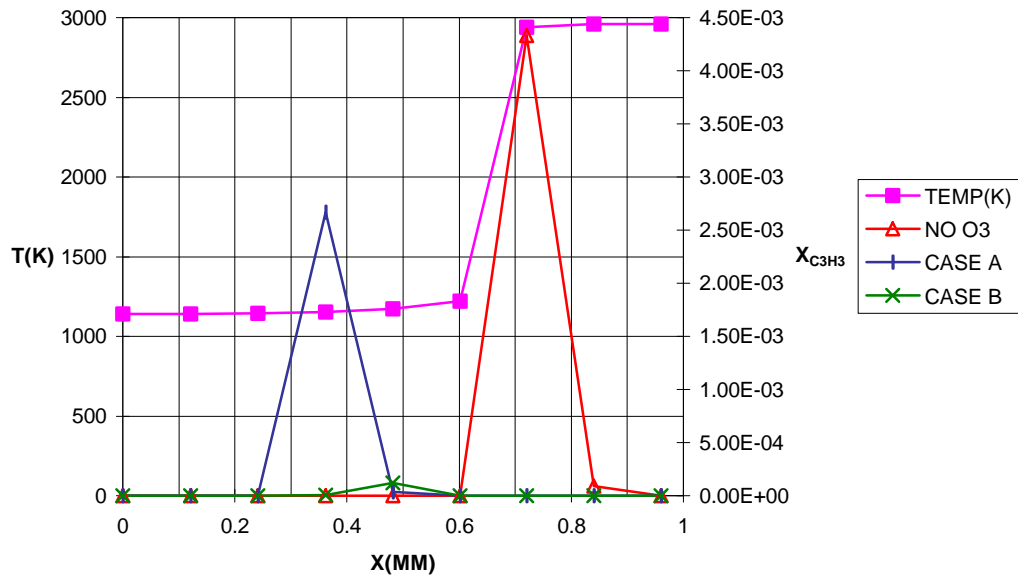


Figure 4.43: The temperature of the no ozone case and concentration of  $C_3H_3$  as a function of position in the expansion stroke at an engine speed of 2500 rpm. Ozone level injected 1000 PPM and all injection times are displayed. Trends shown start at top dead center and end shortly after ignition.

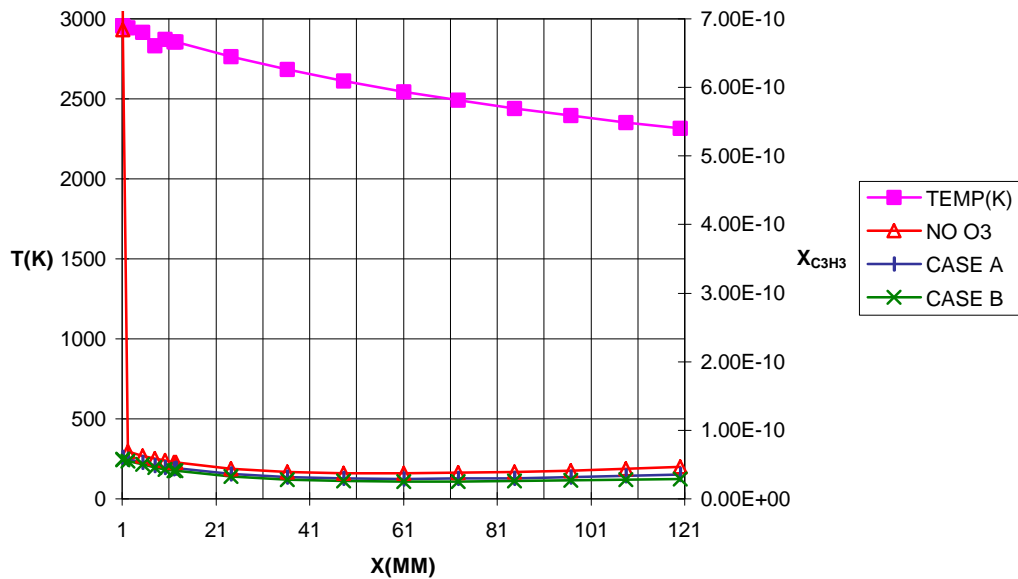


Figure 4.44: The concentration of  $C_3H_3$  as a function of position in the expansion stroke at an engine speed of 2500 rpm. Ozone level injected 1000 PPM and all injection times are displayed. Trends shown start shortly after ignition and end at bottom dead center.

### 4.3 Conclusions

The Senkin program was used to get a better understanding of the chemical kinetics of a diesel engine. The chemical analysis supported several hypotheses on how ozone affects the formation of soot, in addition to how the diesel engine environment directly affect the chemical kinetics. The information obtained from this computational analysis may be summarized as the following:

- 1) Ozone injection does indeed have the potential to reduce soot precursors.
- 2) The injection of ozone in the diesel engine is effective at both speeds.
- 3) Ozone should be injected at the beginning of the expansion stroke.
- 4) The ozone level of 25 PPM is all that is needed to produce an efficient amount of OH to delay the formation of soot precursors.
- 5) Ozone injection decreased ignition time.
- 6) The increase in the soot precursors concentration after ignition is negligible because the generated amount is very small compared to the amount formed at ignition.

## Chapter 5: PSR Analysis

PSR is a program written in Fortran used to model well-stirred reactors. PSR is an acronym that stands for Perfectly Stirred Reactor. This reactor is an adiabatic chamber with one or more inlets and outlets. A perfectly stirred reactor has no species or temperature gradient. The conversion from reactants to products is only controlled by the chemical reaction rates.

Several assumptions are made during the use of this code. The control volume is assumed to be perfectly mixed and homogenous in composition. The reactor is adiabatic and it is modeled for steady state and steady flow conditions. The mass flow rate is characterized by the residence time. This code was used initially because it is an inexpensive and easy aid to understanding combustion pollutants formation. In the end, the predictions of this code were not useful since it precludes the existence of temperature and species gradients.

### 5.1 Formulation

PSR is written in two major modules, TWOPNT and PSR- specific coding. TWOPNT is a code that solves the system of non linear equations describing the perfectly stirred reactor. The PSR - specific coding reads input from the user, call TWOPNT, and solves the solution to generate output. Like the Senkin code, PSR is used in combination with CHEMKIN which is utilized to evaluate the chemical reaction mechanism. The conjunction of these two codes formulate three different output files which generates a synopsis of the chemical analysis. The synopsis that is produced examines level of reactants and products as a function of the residence time.

Unlike the Senkin simulation, PSR was used to only model the expansion stroke. The initial temperature and pressure of compression stroke were not high enough to initiate any chemical reaction. The initial temperature and pressure of the expansion stroke were assumed to be the same temperature and pressure of the Senkin expansion stroke at the different speeds.

The user input describes the reactor. This description includes all parameters needed to solve the chemical reaction mechanism. The simulation of the compression ignition engine require the following parameters: 1) fuel type = hexane ( $C_6H_{14}$ ); 2) initial temperature and pressure of the reactor:  $P_{1500} = 80.3$  atm and  $T_{1500} = 1050$  K;  $P_{2000} = 91.3$  atm and  $T_{2000} = 1098$  K;  $P_{2500} = 103$  atm and  $T_{2500} = 1147$  K; 3) engine speed = 1500, 2000, and 2500 rpm; 4) level of ozone = range from 0 to 1000 ppm; 5)  $\tau$  = residence time which is function of the engine speed; 6) volume of the reactor = 980 ml. The same eleven species analyzed in Senkin were analyzed in PSR.

The mass flow rate is another parameter needed and was inversely proportional to the residence time. As a result, the concept of mass conservation for the individual species becomes

an important factor. The continuity equation for an arbitrary species  $i$  is shown in equation (E5.1) below. (Turns, 1996)

$$dm_{i,cv}/dt = m_i'''V + m_{i,in} - m_{i,out} \quad (E5.1)$$

$dm_{i,cv}/dt =$	Rate at which mass of $i$ accumulates within CV (this term is zero because steady state operations were assumed.)
$m_i'''V =$	Rate at which mass of $i$ is generated within CV
$m_{i,in} =$	Mass flow of $i$ into CV
$m_{i,out} =$	Mass flow of $i$ out of CV

The continuity equation has an additional term ( $m_i'''$ ) which stems from the formation or destruction of a species. This generation term, which is sometimes called source or a sink, is related to the net production rate of the arbitrary species,  $\omega$ . The mass flow rate at the low engine speed (1500 rpm) was 5.90E+02 gm/sec while the higher engine speed (2500 rpm) was 1.22E+03 gm/sec. Since steady state conditions are assumed, the outlet concentrations were equal to the concentrations within the reactor.

## 5.2 Results and Discussion

**Concentration trends of H<sub>2</sub>O and H<sub>2</sub>.** H<sub>2</sub>O is a complete combustion product; while, H<sub>2</sub> is an intermediate that is formed between the decomposition of the fuel and the formation of H<sub>2</sub>O. These species were barely affected by the change in speed or the different levels of ozone. The actual trends of these species are shown in Figure 5.1 - 5.2.

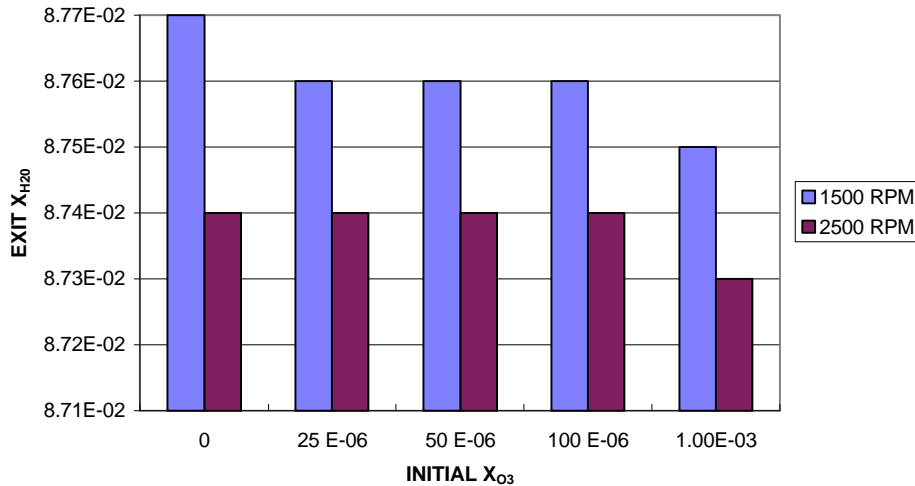


Figure 5.1: The concentration of H<sub>2</sub>O as a function of the initial concentration of ozone at engine speeds of 1500 and 2500 rpm. The four ozone levels displayed are 0, 25, 100, and 1000 ppm.

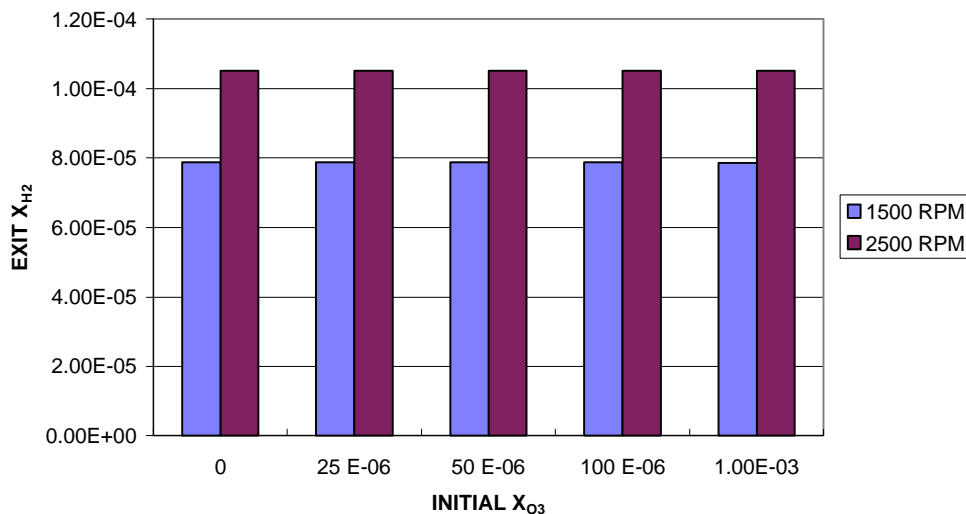


Figure 5.2: The concentration of H<sub>2</sub> as a function of the initial concentration of ozone at engine speeds of 1500 and 2500 rpm. The four ozone levels displayed are 0, 25, 100, and 1000 ppm.

**Concentration of CO<sub>2</sub> and CO.** The oxidation of hexane by ozone leads to the production of carbon species. This analysis will only analyze CO<sub>2</sub> and CO. These carbon species were an immediate result of aromatic ozonation and their evolution was a direct consequence of the attack of the soot and oxidation of intermediate products.

In the PSR simulations, the effect of speed demonstrated different outcomes on these carbon species. When comparing the low and high speed results, a 30% increase in the CO levels was recognized at the high speed; while, the concentration of CO<sub>2</sub> displayed a 2% decrease at the high speed. These trends can be seen in Figure 5.4 and 5.5.

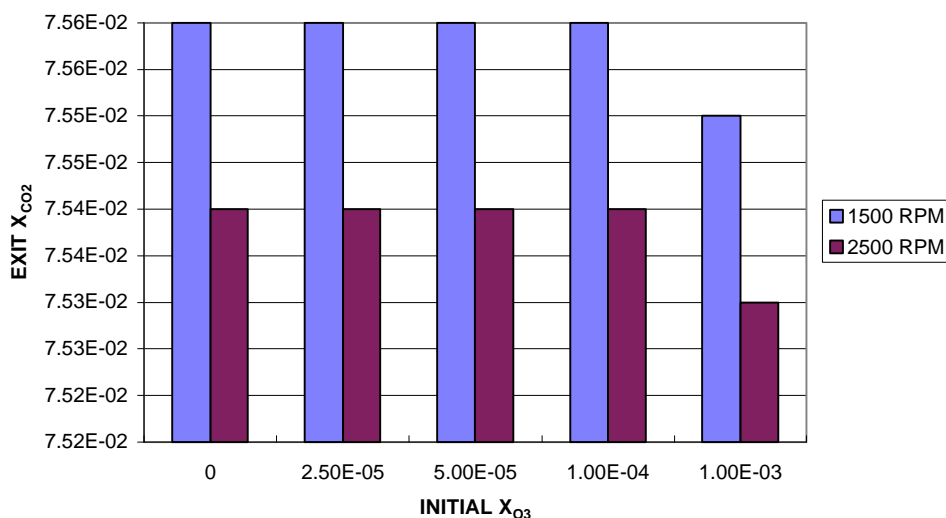


Figure 5.3: The concentration of CO<sub>2</sub> as a function of the initial concentration of ozone at engine speeds of 1500 and 2500 rpm. The four ozone levels displayed are 0, 25, 100, and 1000 ppm.

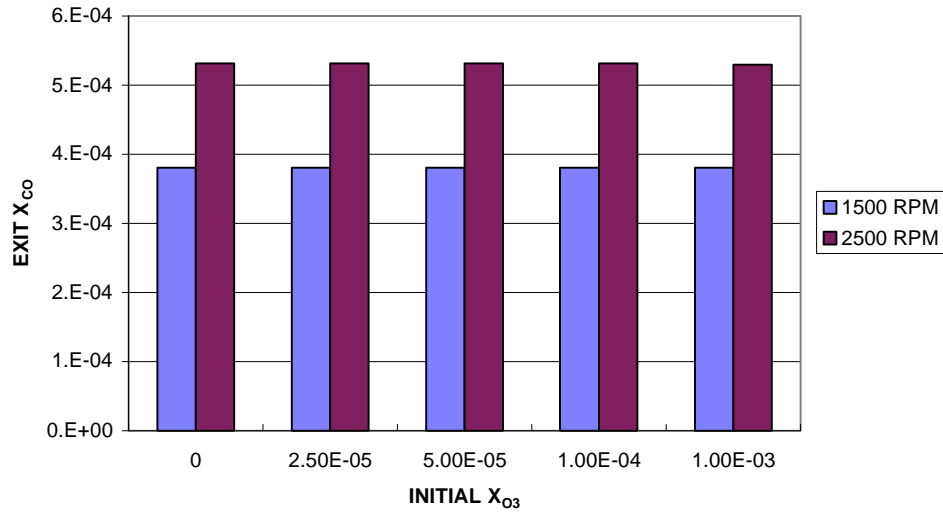


Figure 5.4: The concentration of CO as a function of the initial concentration of ozone at engine speeds of 1500 and 2500 rpm. The four ozone levels displayed are 0, 25, 100, and 1000 ppm.

The different ozone levels slightly altered the concentration of the carbon species. The quantities of the CO and CO<sub>2</sub> were the same for ozone levels of 0 - 100 ppm and only dropped slightly at 1000 ppm.(See Figure 5.3 and 5.4)

**Concentration of O<sub>3</sub>, O<sub>2</sub>, and O.** When ozone decomposes, it forms O<sub>2</sub> and O molecules. The ozone decomposition temperature is approximately 800K. Since, the reactor temperature was much greater than 800 K (approximately 2329 K at 1500 rpm and 2405 K at 2500 rpm) ozone decomposed immediately. Therefore, exit O<sub>3</sub> levels were nearly zero. The exit O<sub>3</sub> concentration is higher at the higher engine speed due to the higher mass flow rate.(See Figure 5.5) However, regardless of the initial level of ozone, the exit quantities were the uniform. Only an 6.47% increase was seen when comparing the no ozone case to 1000 ppm case at the lower engine speed. The comparison percentage between the two levels was 6.07 at the higher engine speed.

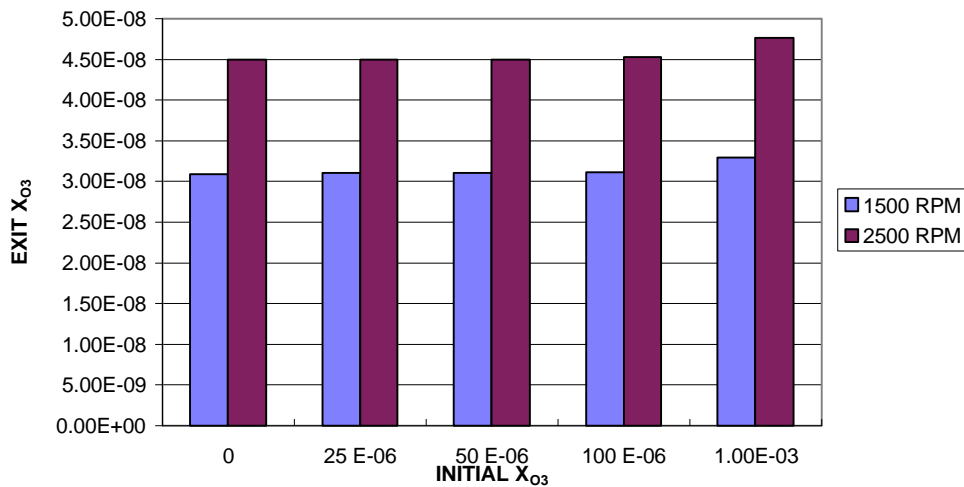


Figure 5.5: The concentration of O<sub>3</sub> as a function of the initial concentration of ozone at engine speeds of 1500 and 2500 rpm. The four ozone levels displayed are 0, 25, 100, and 1000 ppm.

The quantities of O<sub>2</sub> did not change. Therefore, the amount of O<sub>2</sub> formed during the decomposition of O<sub>3</sub> is very small compared to the amount that existed in air. This result was obvious regardless of the level of ozone or engine speed used. (See Figure 5.6)

As seen in Figure 5.7, the level of O increases when speed increases because the rate at which it was being formed was faster at the higher speed. The exit amount of O generated was not significantly influenced by the different levels of ozone used.

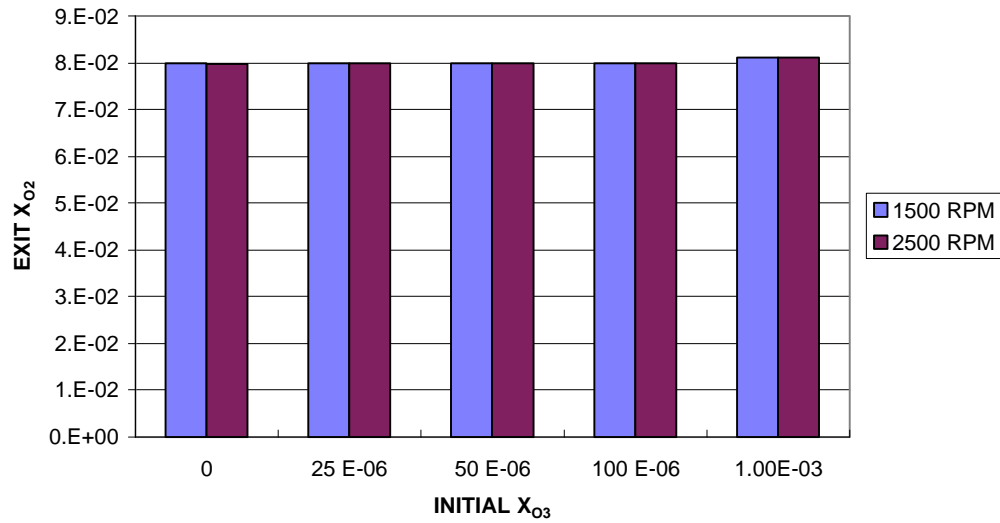


Figure 5.6: The concentration of  $O_2$  as a function of the initial concentration of ozone at engine speeds of 1500 and 2500 rpm. The four ozone levels displayed are 0, 25, 100, and 1000 ppm.

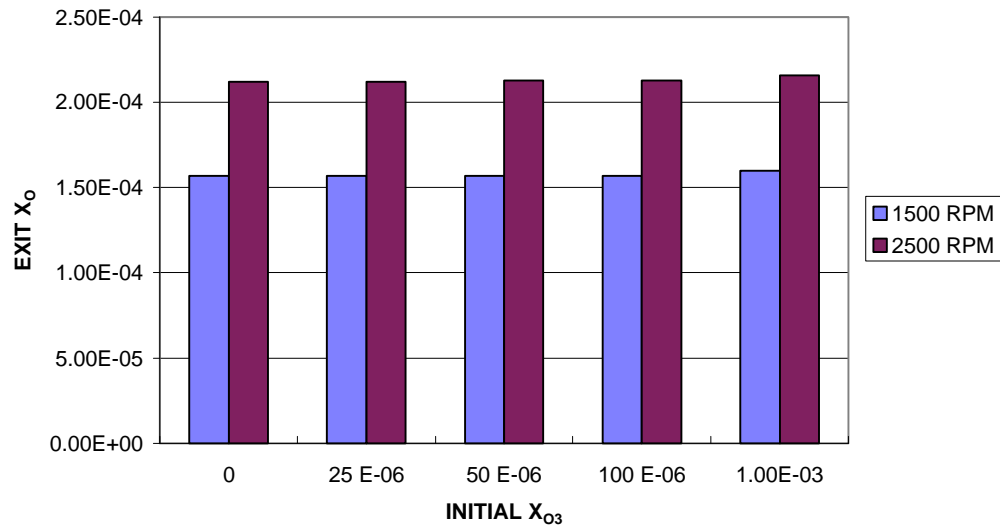


Figure 5.7: The concentration of  $O$  as a function of the initial concentration of ozone at engine speeds of 1500 and 2500 rpm. The four ozone levels displayed are 0, 25, 100, and 1000 ppm.

**Concentration of H.** Monatomic hydrogen is a soot constituent that subjoins with acetylene to form vinylacetylene. Vinylacetylene is one of the initial species formed that leads to the formation of benzene. The exit quantities of H were fairly constant throughout the analysis.

The analysis output exhibited the exit H quantities to be uniform. The H levels were fairly constant regardless of the level of ozone at the different engine speed. However, there was a 49% increase in the H levels at the higher engine speed when contrasting the two speeds. (See Figure 5.8) The generation of H was of a higher order of magnitude than the soot precursors ( $C_2H_2$  and  $C_3H_3$ ). This was probably a consequence of the lower dissociation energy needed to produce the H radicals; hence, making the H radical an easier product to produce.

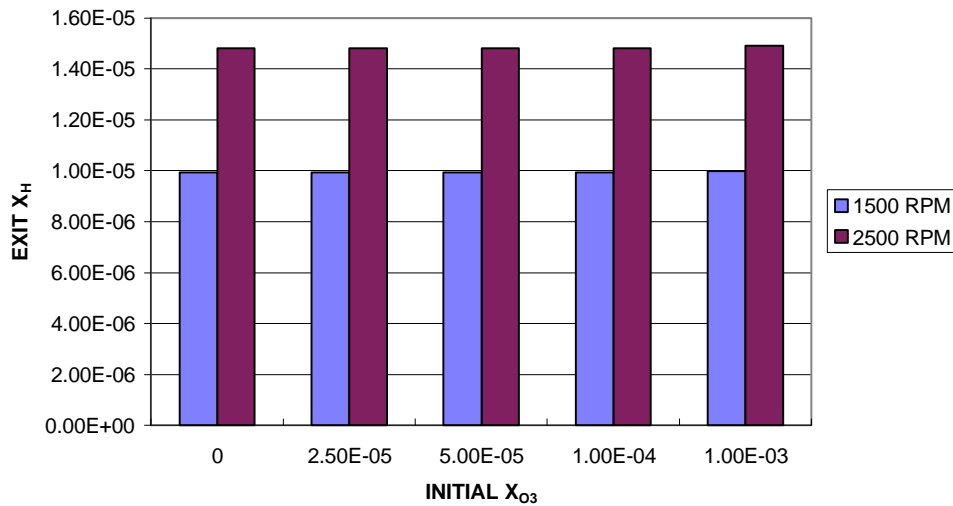


Figure 5.8: The concentration of H as a function of the initial concentration of ozone at engine speeds of 1500 and 2500 rpm. The four ozone levels displayed are 0, 25, 100, and 1000 ppm.

**Concentration of OH.** The formation of soot precursors can be delayed by a strong oxidizer like the OH radical. The concentration of OH is generated from the fuel pyrolysis since the reactor temperature is above 900 K.

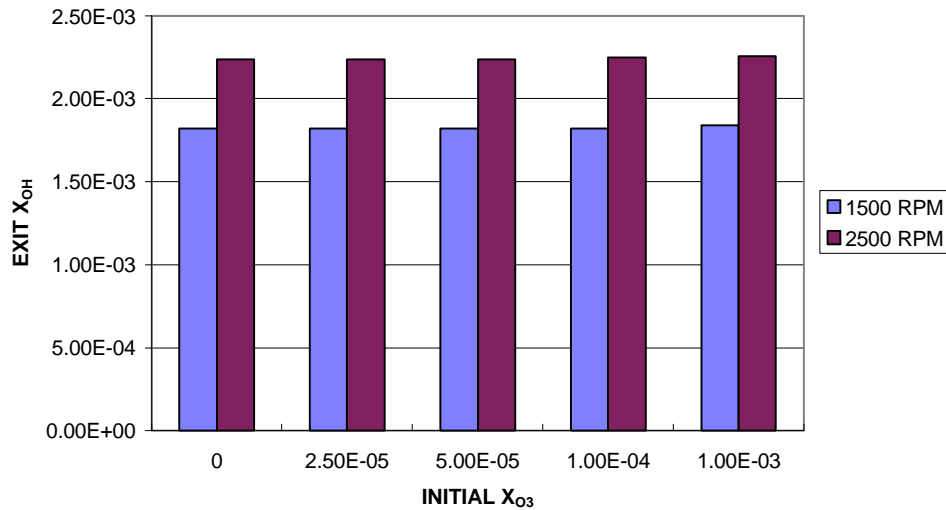


Figure 5.9: The concentration of OH as a function of the initial concentration of ozone at engine speeds of 1500 and 2500 rpm. The four ozone levels displayed are 0, 25, 100, and 1000 ppm.

An examination of the exit conditions reveals, several important features as seen in Figure 5.9. There was a 23% increase in the exit levels of OH at the high engine speed when compared with the low engine speed. The OH generation rate was higher at higher speed which will produce more OH. However, the level of OH was minimally affected by the ozone levels which is evident because exit levels are unchanged. When comparing the no ozone case to the 1000 ppm case, the contrast displayed less than an one percent increase in the OH level. (See Figure 5.9) So, the ozone level used had no effect on the OH production.

**Concentration of C<sub>2</sub>H<sub>2</sub>.** C<sub>2</sub>H<sub>2</sub> is a key contributor to soot formation. C<sub>2</sub>H<sub>2</sub> is the dominant growth species once soot inception has occurred due to its high concentration (Sidebotham and Glassman, 1992). C<sub>2</sub>H<sub>2</sub> is formed at temperatures ranging for 1300K to 2300K (Goldberg, 1985).

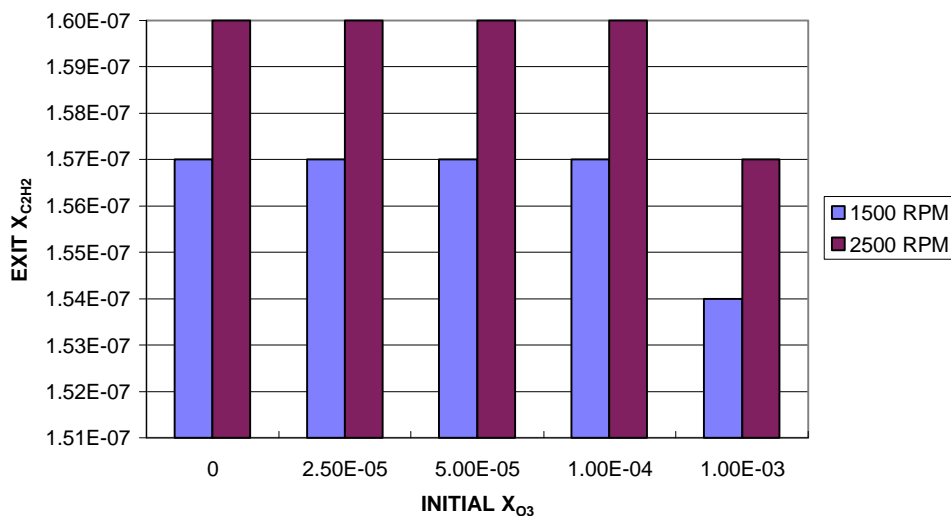


Figure 5.10: The concentration of C<sub>2</sub>H<sub>2</sub> as a function of the initial concentration of ozone at engine speeds of 1500 and 2500 rpm. The four ozone levels displayed are 0, 25, 100, and 1000 ppm.

Uniform data was discovered when analyzing the output results. The engine speed had a minimal effect on the exit C<sub>2</sub>H<sub>2</sub> concentration. There was only a 2% increase in the exit levels when contrasting the speed. ( See Figure 5.10) Ozone levels of 0 - 100 ppm yields the same concentration at both speeds. Although, it was demonstrated that there was a little decrease of 2% in the C<sub>2</sub>H<sub>2</sub> level at 1000 ppm.

**Concentration of  $C_3H_3$ .**  $C_3H_3$  is a highly reactive soot precursor.  $C_3H_3$  is a dominant soot contributor due to the fact it has no weak bonds and the recombination reactions are reversible. During the PSR investigation, uniform trends were again detected. The  $C_3H_3$  level at the 2500 rpm was 20% higher than at 1500 rpm. It was also observed that  $C_3H_3$  level was unaltered by the different ozone levels at the lower engine speed. Identical trends were noticed for the 2500 rpm data, although the  $C_3H_3$  level decreased by 2% at an ozone level of 1000 ppm. (See Figure 5.11)

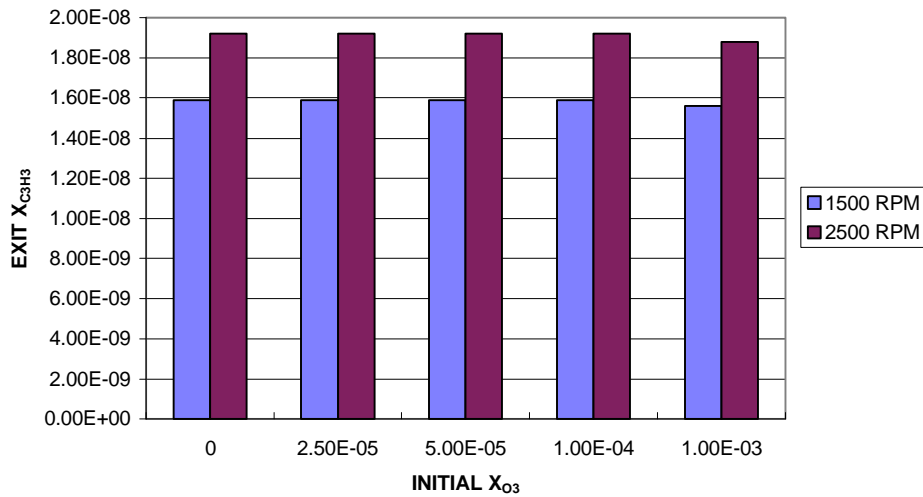


Figure 5.11: The concentration of  $C_3H_3$  as a function of the initial concentration of ozone at engine speeds of 1500 and 2500 rpm. The four ozone levels displayed are 0, 25, 100, and 1000 ppm.

### 5.3 Conclusions

The PSR program was used as an aid to understanding combustion pollutant formation. The chemical analysis contradicted the Senkin analysis results on the effect ozone has on diesel soot precursors. The information obtained from this computational analysis is summarized as follows:

1. In a reactor environment, the higher speed produces more oxidizer than the lower engine.
2. Ozone levels were not an influential factor in the OH production. Therefore, trends did not show a significant decrease in the any exit soot precursor concentrations.
3. PSR predictions were not useful since it precludes the existence of temperature and species gradients.

## Chapter 6. Conclusions

Today's environmentally conscious society has caused emission control to become more of a necessity than a desire. The EPA standards of toxic exhaust emissions continue to decrease year after year. Fuel economy standards are also being reduced. Therefore, finding the means to control the hazardous emissions and increase fuel mileage are influential factors that automobile manufacturers must implement in future vehicles.

The popular solution for increasing fuel mileage is the diesel engine because it is more fuel efficient than the gasoline engine. But with any solution, the benefits will hopefully surpass any tradeoffs. The major tradeoff of the increase use of diesel engines is the lack of an effective way to control emissions. The exhaust fumes from the diesel engines have a harmful effect on the environment because they contribute to air pollution. These exhaust fumes are composed of soot and other particulates which are direct products of unburned hydrocarbons.

In past work, it was found that ozone improved the performance of gasoline engine by reducing exhaust fumes. It was found that the reaction rates of hydrocarbons were greater than the reaction rates of ozone. Therefore, ozone will attack C-H bonds in hydrocarbons. When ozone is added into the air intake at temperatures below 900 K, ozone decomposition and fuel pyrolysis occurred simultaneously generating the  $RO_2$  species. At high temperatures and pressures like those seen in a diesel engine, the  $RO_2$  species become unstable and decompose to form the OH radical. The formation of the OH radicals enhanced the oxidation rate and delayed the inception of soot precursors. These findings stimulated curiosity and initiated a numerical investigation to aid in the understanding of the combustion pollutant formation in the diesel engine.

### 6.1 Conclusions from the Senkin Simulations

The Senkin analysis supported several hypotheses on how ozone affects the formation of soot precursors, in addition to how the diesel engine environment directly affect the chemical kinetics. The information obtained from this computational analysis and previous work may be summarized as follows:

1) Ozone injection does indeed have the potential to reduce soot precursors.

The initial temperature of the expansion stroke was much higher than the ozone decomposition temperature. So when ozone was injected, it decomposed immediately and the chain initiation step of fuel pyrolysis did not result in the formation of alkyl radicals. The decomposition of ozone led to the formation of O atoms and  $O_2$  molecules. These O atoms then bonded with H radicals, formed from cracking reactions, to generate the OH radical. Since the OH radical is an effective

oxidizer, its presence reduced the soot precursor concentration. As the ozone level increased, the OH concentration increased and the soot precursor level decreased.

2) The injection of ozone in the diesel engine is effective at both engine speeds.

All the graphs that displayed the trends starting at top dead center and ending shortly after ignition supported this conclusion. When ozone was injected, the soot precursors concentration at ignition was reduced. The trends seen after ignition are negligible because the concentration of soot precursors were small compared to amount that was produced at ignition.

3) Ozone should be injected at the beginning of the expansion stroke.

When ozone was injected at the beginning of the compression stroke (CASE A), some of the ozone had started to decompose at a temperature of approximately 600K. This early decomposition reduced the amount of reacting ozone available in the expansion stroke. When ozone was injected at the beginning of the expansion stroke (CASE B), there was a larger reduction of the concentration of soot precursors. Therefore, ozone needs to be injected here to have the greatest potential of oxidizing unburned hydrocarbons that stem from the pyrolysis of the combusting fuel.

4) The ozone level of 25 PPM is all that is needed to produce an efficient amount of OH to delay the formation of soot precursors.

When analyzing the percentage increase of OH at the different concentrations of ozone, it was observed that the larger amounts really did not greatly influence the OH level. Since the average ozonator available during research only produces 25 PPM of ozone, its OH percentage was compared with that of 1000 PPM. It was found that 1000 PPM only yields 10% increase in the OH level than 25 PPM. Hence, 25 PPM would clearly be more than enough ozone to produce an effective amount of OH.

5) Ozone injection decreased ignition time.

The burning rate of a hydrocarbon is proportional to the fraction of oxygen available. The no ozone case had the smallest amount of oxygen therefore, the ignition time for this case was a little longer. As a result of this longer time, the initial OH concentration had more time to form during the preliminary reactions that occurs before ignition at the lower injection levels. The largest ignition concentration of OH occurred at the no ozone case.

6) The increase in the soot precursor concentration after ignition is negligible because the generated amount is very small compared to the amount formed at ignition.

The increasing trends seen after ignition resulted from an error in the simulation. These trends are not significant because the minute amount of soot precursors generated after ignition compared to the amount generated at ignition is negligible.

## 6.2 Conclusion from the PSR Simulations

The PSR results contradicted several hypotheses, as well as the results from the Senkin analysis. The information obtained from this computational analysis is summarized as follows:

1. In a reactor environment, the higher speed produces more oxidizer than the lower engine.  
The mixing in the reactor is very intense so the temperature and concentration of the species in the reactor is the same as that which exits the reactor. However, a higher engine speed increases the number of collisions between the reacting molecules; these collisions generated an increase in the reactor temperature. The OH levels were higher at the higher engine speed because the reaction rates were faster.
2. Ozone levels were not an influential factor in the OH production.  
The ozone decomposition temperature is approximately 800K. Since, the reactor temperature was much greater than 800 K (approximately 2329 K at 1500 rpm and 2405 K at 2500 rpm) ozone decomposed immediately. Temperatures are too high for RO<sub>2</sub> complexes to form so the OH concentration is a product of fuel pyrolysis. Therefore, the ozone injection is not an influential factor in OH production. Since the OH radical levels were unchanged, the exit soot precursor concentrations were unaffected by the ozone addition.
3. PSR predictions were not useful since it precludes the existence of temperature and species gradients.  
The steady state assumptions resulted in only one reactor temperature being analyzed. A temperature and species distributions were needed to see where the ignition and the growth and destruction of intermediate species occurred. Therefore, the information gained was not useful.

At the end of these analyses, it became obvious that the PSR analysis was not a good model to use to understand combustion pollutant formation. It was not realized until the conclusion of this simulation that this code was an ineffective aid to understanding combustion pollutant formation because it lacked a temperature and species gradient. The Senkin results exhibited a temperature and species distribution and predicted more realistic results about the ozone injection. However, another computational program is needed to model the actual conditions of a realistic diesel engine. After a realistic simulation is done, its conclusions should agree with the Senkin results.

## Chapter 7: Recommendations for Future Work

The Senkin analysis only varied the ozone levels and engine speeds. To broaden the scope of this analysis, more key factors that control the environment of the diesel engine could be varied. The Senkin analysis could be done using several different fuel-air ratios. This would investigate what fuel-air ratios are the most influenced by the ozone addition. It was found in past work that fuel-air ratios in the range of 0.6 and 0.8 avoided the formation of soot during combustion (Schindler and Hentshel, 1992); therefore, any fuel-air ratio in this range would probably be affected by ozone injection. Another recommendation would be to use several different alkane fuels. Some possible combusting fuel could be heptane, octane, or decane just as long as the skeletal mechanisms for these fuels were used to optimize computational time. The combusting fuel is a major part of soot precursor formation since different fuels use different routes to produce soot.

### 7.1 Use of an additional program

After evaluating the Senkin analysis, the chemical trends of the diesel engine was developed and understood. During this analysis, several ideal boundary conditions were assumed which did not model the diesel engine in a realistic light. The Senkin model utilized a homogenous premixed gas mixture in a closed adiabatic system with a zero dimension. The combusting fuel used in this analysis was hexane. Because of the assumptions of Senkin, an analysis that takes in account the actual conditions of a realistic diesel engine is deemed necessary.

KIVA3 is a computer program that has the ability to calculate flows in engine cylinders with arbitrarily shaped piston geometries and includes the effects of turbulence and wall heat transfer (Amsden, et al., 1989). This program consists of numerous subroutines that work together to numerically calculate transient 2-D and 3-D chemically reactive fluid flows with sprays. Computational fluid dynamics is used to experiment with the design and aid in the understanding of practical combustion systems.

Since KIVA3 was developed with the applications of internal combustion engines in mind, it contains several features designed to facilitate diesel engine applications (Amsden, et al., 1989). The KIVA3 analysis would predict a more practical view of the chemical kinetic behavior of ozone and its effect on the compression ignition engine. Therefore after the completion of this analysis, the actual effect of ozone on diesel soot precursors will be clearly understood.

This simulation will use the applicable conditions of a compression ignited engine. The reacting mixture will be heterogeneous and the combusting fuel will be an actual diesel complex. The diesel complex that could be used in this future analysis would be  $C_{12}H_{26}$ .  $C_{12}H_{26}$  was the diesel fuel model that was fabricated by T. L. McKinley of Cummins Engine Company. The critical temperature, latent heat of vaporization, and liquid viscosity were set equal to those

for n-hexadecane, with the remaining quantities set equal to those for n-dodecane (Amsden, 1993). All four strokes of the diesel engine cycle will be included in this simulation which is different from the initial analyses.

## 7.2 Description of KIVA3

KIVA3 is the latest version of KIVA and is described as a KIVA program with a block-structured mesh for complex geometries. This block-structured mesh has an arbitrary number of logical blocks patched together in a seamless fashion (Amsden, 1993) The four basic block shapes are the piston cup, the squish, the head dome, and all the other cases.

There are five mesh types and the mesh descriptions are given via an user input file. The input file includes the following parameters: the number of vertices, the number of cells, the number of fluid regions, the block shapes, and the instruction for patching blocks together. A block has six bounding faces and initially has its own (i,j,k) structure; although, the block's individual (i,j,k) structure disappears when blocks are patched together. Each cell is identified with a single index and the neighboring cell identification is stored in arrays. The arrayed information specifies the indices of six neighboring cells that share common faces with the cell in question. The overall mesh is surrounded by fictitious cells to simply the application of inflow/outflow boundary conditions (Amsden, 1993).

KIVA3 has a three part structure: the grid generator, the graphics, and the hydro program. The grid generator contains all grid coordinates for the six neighboring arrays, the boundary condition arrays, and the region identifier arrays. The graphics is an output file that illustrates results through zone plots, velocity vector plots, and contour plots. This output file can be used by a graphics post processor to analyze results. The hydro program is an user input file that contains all the desired engine specifications.

The chemical analysis is modified via a subroutine which has the prevalent kinetic and equilibrium chemical data. This chemical data was obtained from several thermodynamic tables. The user determines which species will be evaluated and ensures that the necessary thermodynamic data is in the chemical kinetic subroutine. The species that will be analyzed are :  $C_{12}H_{26}$ ,  $O_2$ ,  $CO_2$ ,  $H_2O$ ,  $H$ ,  $H_2$ ,  $O$ ,  $O_3$ ,  $OH$ ,  $CO$ ,  $C_2H_2$ , and  $C_3H_3$ .

## 7.3 Formulation of KIVA3

Before anything is computed, the initial conditions must be assumed and implemented in the user input file and the boundary condition subroutines. There are several initial conditions which influence the design and the thermodynamics involved in modeling the diesel engine. The crucial conditions are the following: velocity, temperature, pressure, turbulence, density, internal energies, spray injector, cell specifications, and inflow/outflow boundaries. In engine calculations,

the turbulent law of the wall velocity conditions with fixed temperature walls is used for the initial velocity condition (Amsden, 1993). The initial pressure is obtained from time-varying pressure histories which are available from experimental data in most engine applications. The density is determined from the isentropic gas equation of state; and the internal energies are obtained from the pressures and densities used in the equation of state for an ideal gas.

The fuel spray injection model in KIVA3 is sufficiently general, therefore a wide variety of engine injectors or continuous sprays may be specified through input data (Amsden, et al., 1989). The features of the spray injection model include a multiple or multihole nozzle capability and the spray injection types are continuous, solid, or a pulsed hollow cone (Amsden, et al., 1989). The origin, orientation and profile of spray injector is specified in the fuel spray subroutine and includes information about the rotation, thickness of the spray, and mean cone angle. The cell-face boundary conditions are contingent on cell location and cell activity. The possible cell-face boundary conditions are fluid, moving, solid, axis, periodic front, periodic derriere, specified velocity inflow, continutive outflow, pressure inflow and pressure outflow. The inflow boundary is available across the bottom boundary, while the outflow boundary is available across the entire top boundary.

It believed that after the completion of this analysis, the actual effect of ozone on diesel soot precursors would be fully understood. The results of this analysis should agree with the results of Senkin.

## REFERENCES

- Aftel, R., Vandsburger, U., Balakrishnan, G., Roby, R., Frenklach, M., and Kazakov, A., (1995). An Experimental and Numerical Modeling Study of Dual-Mode Counterflow Flames, *Joint Western and Central States Section Meeting of the Combustion Institute*, San Antonio, TX.
- Akhter, M.S., Chughtai, A.R., and Smith, D.M., (1990). Spectroscopic Studies of Oxidized Soots, *Applied Spectroscopy*, 45, p. 653 - 665.
- Alcock, J. and Scott W. (1963). *Some More Light on Diesel Combustion*. Institute of Mechanical Engineers, Automotive Division, p. 179 - 200.
- Amsden, A. A., (1993). *Kiva-3: A KIVA Program with Block-Structured Mesh for Complex Geometries*. Los Alamos National Laboratory report, LA-12503-MS.
- Amsden, A.A., O'Rourke, P.J., Butler, T.D., (1989). *Kiva II: A Computer Program from Chemically Reactive Flows with Sprays*. Los Alamos National Laboratory report, LA-11560-MS.
- Austen, A. and Lyn W. (1961). *Relation between Fuel Injection and Heat Release in a Direct Injection Engine and the Nature of the Combustion Process*. Proceedings Institute of Mechanical Engineers, Automotive Division, p. 47 - 63.
- Balakrishnan, G., (1994). *Innovative Technology for Controlling Soot Emissions from the Diesel Engine*, Proposal, Virginia Polytechnic Institute and State University.
- Balakrishnan, G., (1992). *Effect of Ozone on the Oxidation Rates of Hydrocarbons*, Proposal, University of California San Diego.
- Bechtold, W.E., Dutcher, J.S., Mokler, B.V., Lopez, J.A., Wolf, I., Li, A.P., Henderson, T.R., McClellan, O., (1984). Chemical and Biological Properties of Diesel Exhaust Particles Collected during Selected Segments of Simulated Driving Cycle, *Fundamental and Applied Toxicology*, 4, p. 370 - 377
- Benson, S.W., (1965). Effects of resonance and structure on the thermochemistry of organic peroxy radicals and the kinetics of combustion reaction, *Journal of American Chemical Society*, 87, p. 973 - 979

- Benson, S.W.,(1981). The kinetics and thermochemistry of chemical oxidation with application to combustion and flames. *Progress in Energy and Combustion Science*, 7,p. 125-134.
- Bodner, G.M. and Pardue, H.L.,(1989). *Chemistry: An Experimental Approach*, John Wiley and Sons Inc., New York.
- Docekal, B., Krivan, V. and Pelz, N., (1992). Trace and minor element characterization of diesel soot, *Fresenius Journal of Analytic Chemistry*, 343, p. 873 - 878.
- Donnet, J.B. and Ehrburger, P., and Paprier, E., (1966). *Bull. Soc. Chem.*, 6, p. 2033 - 2038.
- Donnet, J.B. and Ehrburger, P., (1970). *Carbon*, 8, p. 697 -701.
- Donnet, J.B. and Ehrburger, P., and Voet, A., (1972). *Carbon*, 10, p. 737 -740.
- Fridlander, S.K., Altshuler,B., Baynes, K.D., Hackney, J.D., Heck, W.W., McCarroll, J.R., McNesby, J.R., Miller, P.R., Mueller, P.K., Murphy, S.D., (1977). *Ozone and Other Photochemical Oxidants*, National Academy of Sciences, Washington, D.C.
- Glarborg, P., Kee, Robert J., Grar, J.F., Miller, J.A.,(1986). Kinetic, Modeling and Sensitivity Analysis of Nitrogen Oxide Formation in Well- Stirred Reactors, *Combustion and Flame*, 65, p. 177-202.
- Glarborg, P., Kee, Robert J., Grar, J.F., Miller, J.A.,(1992). *PSR: A Fortran Program for Modeling Well - Stirred Reactors*, Sandia National Laboratories, SAND 87-8248.
- Glassman, I., (1987). *Combustion*, Academic Press, Orlando.
- Glassman, I., (1988). Soot Formation in Combustion Processes, *Twenty - Second Symposium (International) on Combustion*, The Combustion Institute.
- Goldberg, Edward, (1985). *Black Carbon in the Environment: Properties and Distribution*, John Wiley and Sons, Inc., New York.
- Hamins, Anthony, (1993). Soot, *Environmental Implications of Combustion Processes*, (ed. I.K. Puri), CRC Press, Chicago, p. 71 - 95.
- Handbook of Chemistry and Physics*, (1992 -1993). p. 5-118 - 5-123
- Haynes, D.S. and Wagner, H.G., (1983). *Progress in Energy and Combustion Science*, 7, p. 229 - 273.

- Holtzclaw, H.F. and Robinson, W.R., (1984). *General Chemistry*, D.C. Heath and Co., Lexington, Mass.
- Hucknall, D.J., (1985). *Chemistry of Hydrocarbon Chemistry*, Chapman and Hall, New York .
- Journal of Phys. Chem. Ref. Data*, (1984). 13, p. 1259 -1380.
- Kuo, K. K. (1986). *Principles of Combustion*, John Wiley and Sons. New York.
- Lee, M.L., Novothy, M., Bartle, K.D.,(1976). *Analyt. Chem.*, 48, p. 1566
- Lutz, Andrew E., Kee, Robert J., Miller, James A.,(1992). *Senkin: A Fortran Program for Predicting Homogenous Gas Phase Chemical Kinetics with Sensitivity Analysis*, Sandia National Laboratories, SAND 87 - 8248.
- Manahan, S.E., (1991). *Environmental Chemistry*, Lewis Publishers, Michigan.
- Miller, J.A. and Melius, C. F., (1992). *Combustion and Flame*, 91, p. 21- 39.
- Obert, Edward F.,(1973). *Internal Combustion Engines and Air Pollution*, Harper and Row Publishers, Inc., New York.
- Otto, M. M., (1898). *Annual Chem. Physics*, 13, p. 109
- Peters, N. and Kee, R.J. (1987). The computation of stretched laminar methane-air diffusion flames using a reduced four-step mechanism, *Combustion and Flame*, 68, p. 17 -23.
- Pollard, R.T. , (1977). Hydrocarbons, *Comprehensive Chemical Kinetics: Gas Phase Combustion*, 17, p. 249 -361.
- Ross, M.M, Chedekel, M.R., Risby, T.H., Lestz, S.S., Yasbin, R.E., (1982). Electron Paramagnetic Resonance Spectrometry of Diesel Particulate Matter, *Environmental International*, 7, p. 325 -329.
- Saito, K., Gordon, A.S., Williams, F. A., and Stickle, W. F., (1991). *Combustion Science and Technology*, 80, p. 103.
- Scheepers, P. T. J. and Bos, R. P., (1992). Combustion of Diesel Fuel from a Toxicological Perspective, *International Archives of Occupational Environmental Health*, 64, p.149 - 161.
- Schindler, K. P. and Hentschel, W., (1992). *Combusting Flow Diagnostics*, 16, p. 439 - 454.

- Sergides, C.A., Jassim, J.A., Chughtal, A. R., and Smith, D.M.,(198 ). The Structure of Hexane Soot Part III: Ozonation Studies, *Applied Spectroscopy*, 41, p. 481 - 492.
- Seshadri, K., Mauss, F., Peter, N., and Warantz, J., (1991) *Twenty - Third Symposium (International) on Combustion*, The Combustion Institute, p. 559
- Sidebotham, G.W. and Glassman, I., (1992). *Combustion and Flame*, 90, p. 269 - 283
- Smith, D.M., Akhter, J.A., Jassim, Sergides, C.A., Welch, W.F., Chughatai, A.R., (1989). Studies of the Structure and Reactivity of Soot, *Applied Science and Technology*, 10, p.311- 325.
- Smith, D.M., Welch, W.F., Jassim, J.A., Chughtah, A.R., (1988). Soot-Ozone Reaction Kinetics: Spectroscopic and Gravimetric Studies, *Applied Spectroscopy*, 42, p. 1473
- Stein, S.E., Walker, J.A., Suryan, M.M., and Fahr, A., (1991). *Twenty - Third Symposium (International) on Combustion*, The Combustion Institute, p. 85.
- Taylor, Charles Fayette, (1968). *The Internal Combustion Engine in Theory and Practice Volume II: Combustion, Fuels, Materials, Design, Mass*, The M.I.T. Press.
- Turns, S.R., (1996). *An Introduction to Combustion: Concepts and Applications*, McGraw Hill, Inc., New York.
- Van Vaeck, L., and Cauwenberghe, K.,(1984). Conversion of Polycyclic Aromatic Hydrocarbon on Diesel Particulate Matter Upon Exposure to Part Per Million Levels of Ozone, *Atmospheric Environment*, 18, p. 323- 328.
- Van Wylen, G. J., and Sonntag, R.E.,(1986). *Fundamentals of Classical Thermodynamics*, John Wiley and Sons, New York.
- Vogl, G. and Elstner, E., F., (1989). Diesel soot particles catalyze the production of oxy-radicals, *Toxicology Letters*, 47, p. 17 - 23.
- Warantz, J.,(1981). Chemistry of Stationary and Nonstationary combustion, *Chemical Physics*, 18, p. 162 - 188.
- Westbrook, C. K., Pitz, W. J., and Leppard, W.R., (1991). *The autoignition chemistry of paraffinic fuel and pop-knock and antiknock additives: A detailed chemical kinetic study*, SAE Paper 912314.

Whitten, K. W. and Gailey, K.D. (1981). *General Chemistry with Qualitative Analysis*, Saunders College Publishing, Philadelphia.

Zierok, K.H., (1981). Ph D Dissertation D 83, Technical University of Berlin.

Zumdahl, S.S., (1989). *Chemistry*, D.C. Heath and Co., Lexington, Mass.

## APPENDIX A: Senkin input file for the expansion stroke. (Case A)

VTIM	<b>Volume is a function of time</b>
PRES 80.4	<b>Initial pressure of expansion stroke (final pressure of the compression stroke).</b>
TEMP 1050	<b>Initial temperature of expansion stroke (final temperature of the compression stroke).</b>
TIME 2E-3	<b>Time of the stroke (depends on engine speed).</b>
DELT 2E-5	<b>Time interval</b>
REAC n2 .790	<b>Mole fraction of N<sub>2</sub> after the compression stroke</b>
REAC o2 .210	<b>Mole fraction of O<sub>2</sub> after the compression stroke</b>
REAC o 6.75E-04	<b>Mole fraction of O after the compression stroke</b>
REAC o3 3.42E-04	<b>Mole fraction of O<sub>3</sub> after the compression stroke</b>
REAC nc6h14 .0368	<b>Mole fraction of C<sub>6</sub>H<sub>14</sub></b>
END	

## APPENDIX B: Senkin input file for the expansion stroke. (Case B)

VTIM	<b>Volume is a function of time</b>
PRES 80.4	<b>Initial pressure of expansion stroke (final pressure of the compression stroke).</b>
TEMP 1050	<b>Initial temperature of expansion stroke (final temperature of the compression stroke).</b>
TIME 2E-3	<b>Time of the stroke (depends on engine speed).</b>
DELT 2E-5	<b>Time interval</b>
REAC n2 .790	<b>Mole fraction of N<sub>2</sub> after the compression stroke</b>
REAC o2 .210	<b>Mole fraction of O<sub>2</sub> after the compression stroke</b>
REAC o3 25E-06	<b>Mole fraction of O<sub>3</sub> after the compression stroke</b>
REAC nc6h14 .0368	<b>Mole fraction of C<sub>6</sub>H<sub>14</sub></b>
END	

## APPENDIX C: Reaction Scheme for Ozone

$(k = A T^{**b} \exp(-E/RT))$

<u>Reaction</u>	A	b	E
O+O <sub>2</sub> +M=O <sub>3</sub> +M N <sub>2</sub> /1.0/ O <sub>2</sub> /0.4/	1.78E21	-2.8	0.0
O <sub>3</sub> +O=2O <sub>2</sub>	4.818E12	0.0	4.090E6

## APPENDIX D: Volume as a function of time (Senkin Simulation)

Since the volume is a specified function of time, a subroutine must be provided to return the volume and its time derivative. The subroutine has this form

### SUBROUTINE VOLT (TIME, VOL, DVDT)

The units of time are in seconds and time is given in the user input file. The units of volume are in  $\text{cm}^3$ . This subroutine can be found in the driver program of Senkin and was modified using the equations listed below.

#### Compression stroke

$$V(t)_{1500 \text{ rpm}} = -4903(t) + 1040 \quad \text{cm}^3 \quad 0 \leq t \leq 0.02$$

#### Expansion stroke

$$V(t)_{1500 \text{ rpm}} = +4903(t) + 59.4 \quad \text{cm}^3 \quad 0.02 \leq t \leq 0.04$$

$$\frac{Dv}{Dt} = \pm 4903 \text{ cm}^3$$

#### Compression stroke

$$V(t)_{2000 \text{ rpm}} = -65.3E03(t) + 1040 \quad \text{cm}^3 \quad 0 \leq t \leq 0.015$$

#### Expansion stroke

$$V(t)_{2000 \text{ rpm}} = +65.3E03(t) + 59.4 \quad \text{cm}^3 \quad 0.015 \leq t \leq 0.03$$

$$\frac{Dv}{Dt} = \pm 65.3E03 \text{ cm}^3$$

#### Compression stroke

$$V(t)_{2500 \text{ rpm}} = -8.17E03(t) + 1040 \quad \text{cm}^3 \quad 0 \leq t \leq 0.012$$

#### Expansion stroke

$$V(t)_{2500 \text{ rpm}} = +8.17E03(t) + 59.4 \quad \text{cm}^3 \quad 0.012 \leq t \leq 0.024$$

$$\frac{Dv}{Dt} = \pm 8.17E03 \text{ cm}^3$$

**Example:**

SUBROUTINE VOLT (A, B, C)

(A = TIME; B = VOL; C = DVDT)

IMPLICIT DOUBLE PRECISION (A-H, O-Z)

B = (8.17D03 \* A ) + 59.4

C = 8.17D03

RETURN

END

## **VITA**

### **Inga L. Faison**

Inga L. Faison was born on November 10, 1971 in Norfolk, Va., to Louis and Veta Faison. During her childhood, her father always stressed how she should be a well-rounded woman that knows a little about everything. Therefore, every time he fixed something on the car or anything else for that matter, he made sure she understood what he was doing and why. From this exposure and her great love of math, led her to pursue two degrees in Mechanical Engineering.

She obtained her Bachelor's of Science in Mechanical Engineering in May 1994, from VA Tech. She then worked at AT&T in Richmond, VA as an Engineering intern and returned to VA Tech to pursue her Master's degree in Mechanical Engineering in January 1995. During the summer of 1995, she went back to Richmond to work as a summer intern for ABB (Asea Brown Boveri). Now, in May 1997 she graduated from VA Tech a second time with a Master's degree in Mechanical Engineering. After graduation, she plans to work for DuPont in Nashville as a Manufacturing Engineer.

The Master's degree was a stepping stone to her ultimate goal of eventually obtaining a doctorate degree. After which she plans to work in industry for a while and later become a college professor.